PHYSICAL REVIEW D **86,** 054505 (2012)

Restoration of rotational symmetry in the continuum limit of lattice field theories

Zohreh Davoudi[1,*] and Martin J. Savage[1,†]

[1]*Department of Physics, University of Washington, Box 351560, Seattle, Washington, DC 98195, USA*

(Received 27 May 2012; published 12 September 2012)

We explore how rotational invariance is systematically recovered from calculations on hyper-cubic lattices through the use of smeared lattice operators that smoothly evolve into continuum operators with definite angular momentum as the lattice-spacing is reduced. Perturbative calculations of the angular momentum violation associated with such operators at tree level and at one loop are presented in $\lambda\phi^4$ theory and QCD. Contributions from these operators that violate rotational invariance occur at tree-level, with coefficients that are suppressed by $\mathcal{O}(a^2)$ in the continuum limit. Quantum loops do not modify this behavior in $\lambda\phi^4$, nor in QCD if the gauge-fields are smeared over a comparable spatial region. Consequently, the use of this type of operator should, in principle, allow for Lattice QCD calculations of the higher moments of the hadron structure functions.

DOI: 10.1103/PhysRevD.86.054505 PACS numbers: 12.38.Gc, 11.15.Ha

I. INTRODUCTION

Lattice quantum chromodynamics (LQCD) is a numerical technique in which Euclidean space correlation functions of QCD are calculated by a Monte-Carlo evaluation of the Euclidean space path integral [1]. The computational resources are now becoming available for LQCD to recover the spectrum of mesons and baryons that have been observed in the laboratory, and to make predictions of states with exotic quantum numbers that will be the focus of future experimental efforts. It is also providing precise determinations of the matrix element of weak operators that are required to further constrain the mixing of the eigenstates of the weak interaction contained in the Cabibbo-Kobayashi-Maskawa (CKM) matrix. LQCD is allowing for a comprehensive description of the structure of nucleons, and more recently to their interactions that are crucial to the field of nuclear physics. This marks the beginnings of a comprehensive program to determine nuclear structure and dynamics directly from QCD.

Space-time is pixelated, or discretized, in LQCD calculations, with the quarks residing on the lattice sites, and the gluon fields residing on the links between lattice sites. The lattice spacing, a, the distance between adjacent lattice sites, is required to be much smaller than the characteristic hadronic length scale of the system under study. In principle, the effects of a finite lattice spacing can be systematically removed by combining calculations of correlation functions at several lattice spacings with the low-energy effective field theory which explicitly includes the discretization effects. This type of effective field theory is somewhat more complicated than its continuum counterpart as it must reproduce matrix elements of the Symanzik action constructed with higher dimension operators induced by the discretization [2–4]. While the action lacks Lorentz invariance and rotational symmetry, it is constrained by hyper-cubic symmetry. As computers have finite memory and performance, the lattice volumes are finite in all four space-time directions. Generally, periodic boundary conditions are imposed on the fields in the space-directions (a three-dimensional torus), while (anti) periodic boundary conditions are imposed on the (quark) gauge-fields in the time-direction. However, the conceptual and practical problems arising from the explicit breaking of the space-time symmetries of the continuum theory, down to those of a hyper-cubic lattice theory, remain a challenge in the continuum extrapolation of classes of observables calculated using LQCD. One knows, however, that as the lattice becomes finer, the full space-time symmetries of the continuum are in fact approximately recovered for observables involving wavelengths that are large compared with the scale of pixelation.[1] As a result, a quantitative description of this restoration, as well as its implication for calculation of lattice observables, is possible.

Efforts to reduce lattice artifacts and achieve a better behaved theory in the continuum limit date back to the early stages of development of LQCD. Many that fall under the name of Symanzik improvement include a systematic modification of the action in such a way to eliminate $\mathcal{O}(a^n)$ terms from physical quantities calculated with LQCD at each order in perturbation theory [2–4,8–15], or nonperturbatively. However, as will be discussed, discretization effects are known to give rise to more subtle issues; the treatment of which turns out to be more involved. LQCD is commonly formulated on a hyper-cubic grid, as a result the full (Euclidean) Lorentz symmetry group of the continuum is reduced to the discrete symmetry group of a hyper-cube. As the (hyper-) cubic group has only a finite number of irreducible representations (irreps) compared to

*davoudi@uw.edu
†savage@phys.washington.edu

[1]For some numerical illustrations of this recovery in $SU(2)$ lattice gauge theories, as well as the scalar ϕ^4 theory, see Refs. [5–7].

infinite number of irreps of the rotational group, a given irrep of the rotational group is not irreducible under the (hyper-) cubic group. Consequently, one cannot assign a well-defined angular momentum to a lattice state, which is generally a linear combination of infinitely many different angular momentum states (see for example Refs. [16–18]). In principle, one can identify the angular momentum of a corresponding continuum state in a lattice calculation from the degeneracies in the spectrum of states belonging to different irreps of the cubic group as the lattice spacing is reduced (a review of baryon spectroscopy efforts is given in Ref. [19], for some recent meson spectroscopy works see Refs. [20–23]). However, as the density of degenerate states substantially increases with increasing the angular momentum, the identification of states with higher angular momentum becomes impossible with the current statistical precision. The other issue is that the cubic symmetry of the lattice allows the renormalization mixing of interpolating operators with lower dimensional ones. The induced coefficients of the lower-dimensional operators scale as inverse powers of the lattice spacing, and hence diverge as the lattice spacing goes to zero. Although renormalization mixing of operators is familiar from the continuum quantum field theory, it happens more frequently in LQCD calculations as the reduced symmetry of the hyper-cube is now less restrictive in preventing operators from mixing. To obtain useful results for, as an example, the matrix elements of operators from LQCD calculations, nonperturbative subtraction of the power-divergences is required and generally introduces large statistical uncertainties.

To overcome these obstacles, it has been recently proposed by Dudek, *et al.* [24–26] (and later applied to bottom-baryon systems by Meinel [27]) that by means of a novel construction of interpolating operators, the excited states of several mesons and baryons can be identified to high precision. The essence of this method is that if one uses a set of cubically invariant local operators which have already been subduced [28] from a rotationally invariant local operator with a definite angular momentum, J, while at the same time smearing the gauge and quark fields over the hadronic scale [29–31], the constructed operator has maximum overlap onto a continuum state with angular momentum J if the lattice spacing is sufficiently small. The subduction is assumed to be responsible for retaining ''memory'' of the underlying angular momentum of the continuum operator, while the smearing is assumed to suppress mixing with operators of different angular momentum by filtering contributions from ultraviolet (UV) modes. In another approach, states with higher angular momentum in the glueball spectra of $2+1$ dimensional $SU(2)$ gauge theories [32,33] are isolated by using glueball interpolating operators that are linear combinations of Wilson loops which are rotated by arbitrary angles in order to project out a particular angular momentum J in the continuum. In addition, the links are smeared, or blocked, in order to be smooth over physical length scales rather than just in the UV [34]. So by monitoring the angular content of the glueball wave function in the continuum limit with a probe with definite J, the $0^-/4^-$ puzzle in the glueball spectroscopy has been tackled. The prominent feature of these works is that the recovery of rotational symmetry for sufficiently small lattice spacings is qualitatively emergent from their numerical results.

The same issue occurs in LQCD calculations of higher moments of hadron structure functions, the extraction of which requires the matrix elements of local operators between hadronic states. Although Lorentz invariance forbids twist-2 operators with different J from mixing in the continuum, generally they can mix in LQCD calculations with power-divergent mixing coefficients [35,36]. The power-divergent mixing problem associated with the lower moments can be avoided by several means as described, for example, in Refs. [36–45]. In addition to these approaches, two methods [46,47] have been suggested that highlight the idea of approaching the continuum properties of the hadronic matrix elements by suppressing the contributions from the UV, and in that sense resemble the idea of operator smearing in the proposals described above. In LQCD calculations of non-leptonic K-decay, Dawson *et al.* [46] suggested that point-splitting the hadronic currents by a distance larger than the lattice spacing, but smaller than the QCD scale, results in an operator product expansion of the currents with the coefficients of lower dimensional operators scaling with inverse powers of the point-splitting distance, as opposed to the inverse lattice spacing. This considerably reduces the numerical issues introduced by the operator mixing. In a different, but still physically equivalent approach, Detmold and Lin [47] showed that in the LQCD calculation of matrix elements of the Compton scattering tensor, the introduction of a fictitious, nondynamical, heavy quark coupled to physical light quarks removes the power divergences of the mixing coefficients. This technique enables the extraction of matrix elements of higher spin twist-2 operators with a simple renormalization procedure. The essence of this method is that the heavy quark propagator acts as a smearing function in the momentum-space, suppressing contributions from the high energy modes, provided that its mass is much smaller than the inverse lattice spacing.

Encouraged by the results of the numerical nonperturbative investigation of Refs. [24–26,32,33], as well as the results of Refs. [46,47], we aim to quantify the recovery of rotational symmetry with analytical, perturbative calculations in $\lambda\phi^4$ and QCD. In order to achieve this goal, we first define a composite operator on the lattice which has a well-defined angular momentum in the continuum limit and is smeared over a finite physical region, and show how the noncontinuum contributions to the multipole expansion of the operator scales as the lattice spacing is reduced toward the continuum. Tree-level contributions to matrix

elements that violate rotational symmetry, either by the lattice operator matching onto continuum operators with the "wrong" angular momentum, or matching onto continuum operators that explicitly violate rotational symmetry, scale as $\mathcal{O}(a^2)$ as $a \to 0$. This includes the (naively) power divergent contributions from lower-dimension operators. In order to make definitive statements about the size of violations to rotational symmetry, it must be ensured that the tree-level scalings are not ruined by quantum fluctuations. This is demonstrated by a perturbative calculation of the two-point function in $\lambda\phi^4$ scalar field theory with an insertion of such an operator. It is confirmed that quantum corrections at any order in perturbation theory do not alter the observed classical scalings of non-continuum contributions. This result is comparable with finite size scaling results of the leading irrelevant operator that breaks rotational invariance in three dimensional $O(N)$ models given in Refs. [48,49]. The critical exponent ρ introduced there has a realization in terms of small-a scaling of the leading rotational invariance violating terms in this calculation. Its value is shown to be consistent with the results presented here.

After gaining experience with this operator in scalar field theory, the generalization to gauge theories is straightforward. Special attention must be paid to the gauge links that appear in the definition of gauge-invariant operator(s) that are the analogue of those considered in the scalar field theory. Also, it is well known that the perturbative expansion of operators used in LQCD are not well-behaved due to the presence of tadpole diagrams [50]. Naively, tadpoles make enhanced contributions to the matrix elements of the operators we consider, and that tadpole improvement of the gauge links and smearing of the gluon fields are crucial to the suppression of violations of rotational symmetry. After discussing the continuum behavior of the QCD operator(s), and their potential mixings, which violate rotational invariance at $\mathcal{O}(a^2)$, we determine the renormalization of the operator(s) on the lattice at one-loop order. The leading rotational invariance violating contributions to the renormalized lattice operator are suppressed by $\mathcal{O}(\alpha_s a^2)$, (where $\alpha_s = g_s^2/(4\pi)$ and g_s is the strong coupling constant) provided that the gauge fields are also smeared over a physical region similar to the matter fields. This means that the leading rotational invariance violating operators introduced by the quantum loops make subleading contributions compared to tree level, $\mathcal{O}(a^2)$. The loop contributions that scale as $\mathcal{O}(\alpha_s a)$ do not violate rotational symmetry, and hence are absorbed into the operator Z-factor.

II. OPERATORS IN SCALAR FIELD THEORY

The goal is to construct a bilinear operator of the scalar fields on a cubic lattice which has certain properties. First of all, as it was discussed earlier, it has to be smeared over a finite region of space. This physical region should be large compared to the lattice spacing, and, for our purposes, small compared to typical length scale of the system to allow for a perturbative analysis. The spatial extent of the operator can be identified with its renormalization scale. Second, it is required to transform as a spherical tensor with well-defined angular momentum in the continuum limit. An operator that satisfies these conditions is[2]

$$\hat{\theta}_{L,M}(\mathbf{x}; a, N) = \frac{3}{4\pi N^3} \sum_{\mathbf{n}}^{|\mathbf{n}|\le N} \phi(\mathbf{x})\phi(\mathbf{x} + \mathbf{n}a) Y_{L,M}(\hat{\mathbf{n}}), \quad (1)$$

where $\mathbf{n}$ denotes a triplet of integers, and it is normalized by the spatial volume of the region over which it is distributed. $\phi(\mathbf{x})$ is the scalar field operator, N is the maximum number of lattice sites in the radial direction, and $Y_{LM}(\hat{\mathbf{n}})$ is a spherical harmonic evaluated at the angles defined by the unit vector in the direction of $\mathbf{n}$, $\hat{\mathbf{n}}$, as shown in Fig. 1. This operator can also be written in a multipole expansion about its center as

$$\hat{\theta}_{L,M}(\mathbf{x}; a, N) = \frac{3}{4\pi N^3} \sum_{\mathbf{n}}^{|\mathbf{n}|\le N} \sum_{k} \frac{1}{k!} \phi(\mathbf{x})(a\mathbf{n}\cdot\nabla)^k \phi(\mathbf{x}) Y_{L,M}(\hat{\mathbf{n}}), \quad (2)$$

where the gradient operator acts on the $\mathbf{x}$ variable, $\nabla \equiv \nabla_{\mathbf{x}}$.

Although the operator $\hat{\theta}_{L,M}(\mathbf{x}; a, N)$ is labeled by its angular momentum in the continuum limit, from the

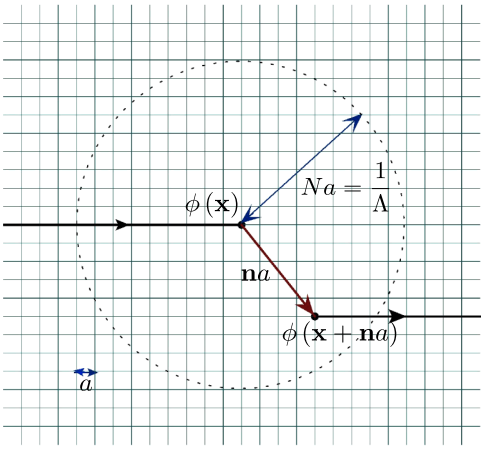

FIG. 1 (color online). A contribution to the lattice operator defined in Eq. (1), with $|\mathbf{n}| \le N$. All the points inside the three-dimensional spherical shell $|\mathbf{n}a| = Na$ are included in the operator. The two length scales defining the operator, the lattice spacing, a, and the operator size, $Na = 1/\Lambda$, are shown.

[2]This corresponds to one particular choice of radial structure of the operator. However, the results of the calculations and the physics conclusions presented in this work do not change qualitatively when other smooth radial structures are employed, such as a Gaussian or exponential.

right-hand side of Eq. (2), it is clear that it is a linear combination of an infinite number of operators with angular momentum compatible with its parity. To be more specific, consider the $M = 0$ component of the operator expanded in a derivative operator basis,

$$\hat{\theta}_{L,0}(\mathbf{x}; a, N) = \sum_{L',d} \frac{C^{(d)}_{L0;L'0}(N)}{\Lambda^d} \mathcal{O}^{(d)}_{z^{L'}}(\mathbf{x}; a), \tag{3}$$

where $\mathcal{O}^{(d)}_{z^{L'}}(\mathbf{x}; a)$ are defined in Appendix A. The operator subscript denotes that there are L' free indices in the derivative operator, while d denotes the total number of derivatives. As is discussed in the Appendix A, there are operators in this basis which are not rotationally invariant but only cubically invariant. $C^{(d)}_{L0;L'0}(N)$ are coefficients of each operator in the expansion whose values are determined by matching Eq. (2) with Eq. (3). Finally $\Lambda = 1/(Na)$ is the momentum-scale of the smeared operator which is kept fixed as the lattice spacing is varied. Therefore, as the lattice spacing decreases, more point shells (shells of integer triplets) are included in the sum in Eq. (2). The convergence of this derivative expansion is guaranteed as the scale Λ is set to be much larger than the typical momentum encountered by the operator.

A. Classical scalar field theory

In order for the operator to recover its continuum limit as the lattice spacing vanishes, the coefficients $C^{(d)}_{L0;L'0}$ should have certain properties. First of all, those associated with the operators with $L \neq L'$ as well as the rotational invariance violating operators, should vanish as $a \to 0$. Also the coefficients of rotational invariant operators with $L = L'$ should reach a finite value in this limit. These properties will be shown to be the case in a formal way shortly, but in order to get a general idea of the classical scaling of the operators and the size of mixing coefficients, we first work out a particular example. Consider the operator $\hat{\theta}_{3,0}(\mathbf{x}; a, N)$ expanded out up to five derivative operators,

$$\begin{aligned}
&\hat{\theta}_{3,0}(\mathbf{x}; a, N) \\
&\quad = \frac{C^{(1)}_{30;10}(N)}{\Lambda} \mathcal{O}^{(1)}_{z}(\mathbf{x}; a) + \frac{C^{(3)}_{30;10}(N)}{\Lambda^3} \mathcal{O}^{(3)}_{z}(\mathbf{x}; a) \\
&\quad + \frac{C^{(5)}_{30;10}(N)}{\Lambda^5} \mathcal{O}^{(5)}_{z}(\mathbf{x}; a) + \frac{C^{(5;\mathrm{RV})}_{30;10}(N)}{\Lambda^5} \mathcal{O}^{(5;\mathrm{RV})}_{z}(\mathbf{x}; a) \\
&\quad + \frac{C^{(3)}_{30;30}(N)}{\Lambda^3} \mathcal{O}^{(3)}_{zzz}(\mathbf{x}; a) + \frac{C^{(5)}_{30;30}(N)}{\Lambda^5} \mathcal{O}^{(5)}_{zzz}(\mathbf{x}; a) \\
&\quad + \frac{C^{(5)}_{30;50}(N)}{\Lambda^5} \mathcal{O}^{(5)}_{zzzzz}(\mathbf{x}; a) + \mathcal{O}\left(\frac{\nabla_z^7}{\Lambda^7}\right),
\end{aligned} \tag{4}$$

where the superscript RV denotes the rotational invariance violating operator and its corresponding coefficient in the above expansion.

The numerical values of the coefficients in Eq. (4), at the classical level, as a function of the maximum shell included in the sum in Eq. (2) are shown in Figs. 2 and 3. From these plots it is clear that while the coefficients $C^{(3)}_{30;30}$ and $C^{(5)}_{30;30}$ reach a finite value for large N, the coefficients of lower and higher angular momentum operators, as well as the rotational invariance violating operator, approach zero. To find the values of the leading order (LO) coefficients in this limit, as well as to see how the nonleading contributions scale with $N = 1/(\Lambda a)$, one can apply the Poisson re-summation formula to the right-hand side of Eq. (2),

$$\begin{aligned}
\hat{\theta}_{L,M}(\mathbf{x}; a, N) = \frac{3}{4\pi N^3} \sum_k \frac{a^k}{k!} \sum_{\mathbf{p}} \int d^3y \theta(N - y) e^{i2\pi \mathbf{p}\cdot\mathbf{y}} \\
\times \phi(\mathbf{x})(\mathbf{y}\cdot\nabla)^k \phi(\mathbf{x}) Y_{L,M}(\hat{\mathbf{y}}),
\end{aligned} \tag{5}$$

where $\mathbf{p}$ is another triplet of integers, and the $\mathbf{p}$ summation is unbounded. The continuum values of the coefficients obtained in the $N \to \infty$ limit, corresponding to the $\mathbf{p} = 0$ term in Eq. (5), are

$$C^{(d)}_{30;30} = \frac{15}{4}\sqrt{\frac{7}{\pi}} \frac{d^2 - 1}{(d+4)!} \quad \text{with} \quad d = 3, 5, \ldots, \tag{6}$$

while the other coefficients in Eq. (4) vanish in this limit as expected. The LO corrections to these continuum values can be calculated as following. The deviation of $C^{(3)}_{30;30}$ from its continuum value can be found from

$$\begin{aligned}
I_{30} \sim \frac{3}{4\pi} \frac{(Na)^3}{3!} \sum_{\mathbf{p}\neq 0} \int_0^1 dy y^2 d\Omega_{\hat{y}} e^{i2\pi N \mathbf{p}\cdot\mathbf{y}} \phi(\mathbf{x})(\hat{\mathbf{y}}\cdot\nabla)^3 \\
\times \phi(\mathbf{x}) Y_{3,0}(\hat{\mathbf{y}}),
\end{aligned} \tag{7}$$

where $\nabla = \nabla_z \hat{e}_z$ and the y-variable in Eq. (7) is redefined to lie between 0 and 1, and it is straightforward to show that

$$\begin{aligned}
\delta C^{(3)}_{30;30} = \frac{1}{N^2} \frac{1}{32\pi^2} \sqrt{\frac{7}{\pi}} \sum_{\mathbf{p}\neq 0} \frac{\cos(2\pi N|\mathbf{p}|)}{|\mathbf{p}|^8} \\
\times \left(-\frac{3}{2}|\mathbf{p}|^6 + 15|\mathbf{p}|^2 p_z^4 - \frac{25}{2} p_z^6\right).
\end{aligned} \tag{8}$$

It is interesting to note that, after trading N for $1/(a\Lambda)$, the finite lattice spacing corrections are not monotonic in a, but exhibit oscillatory behavior, which is clearly evident in Fig. 2.

The deviation of $C^{(1)}_{30;10}$ from its continuum value of zero follows similarly, and is found to scale as $\sim 1/N^2$,

$$\delta C^{(1)}_{30;10} = \frac{1}{N^2} \frac{3}{16\pi^2} \sqrt{\frac{7}{\pi}} \sum_{\mathbf{p}\neq 0} \frac{\cos(2\pi N|\mathbf{p}|)}{|\mathbf{p}|^6} (|\mathbf{p}|^4 - 5p_z^4). \tag{9}$$

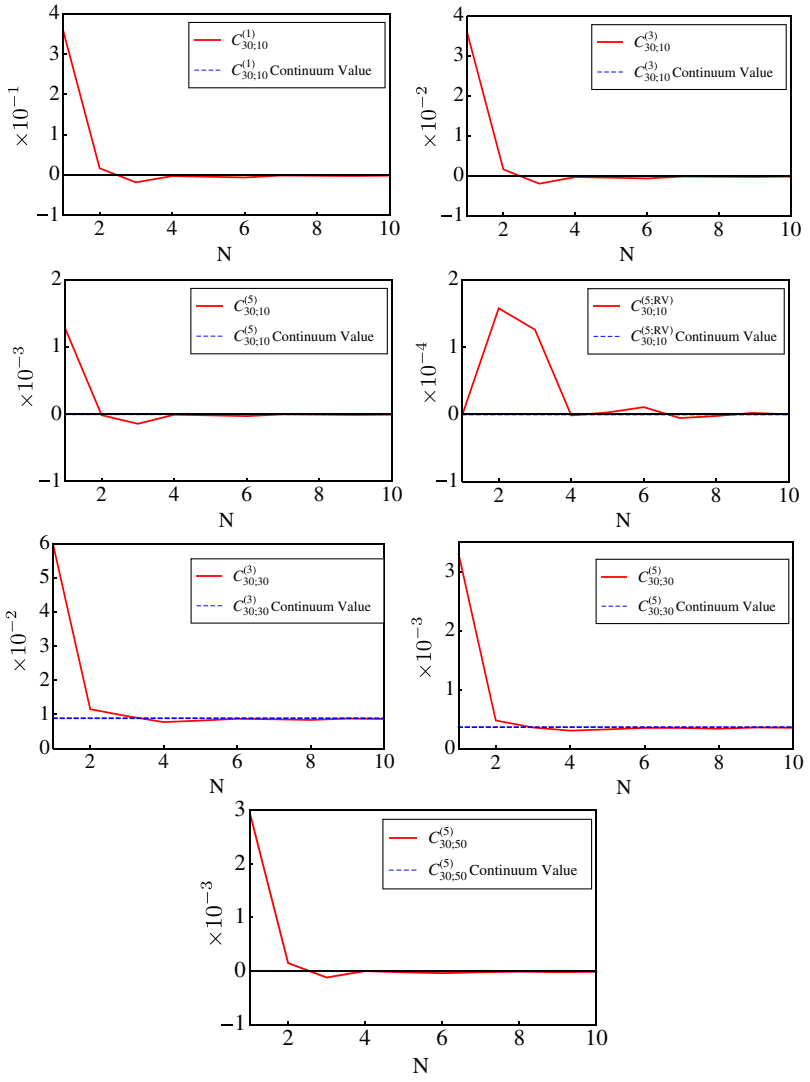

FIG. 2 (color online). The tree-level values of the coefficients $C^{(d)}_{30;L'0}$ appearing in Eq. (4) as a function of the largest n-shell included in the summation in Eq. (1).

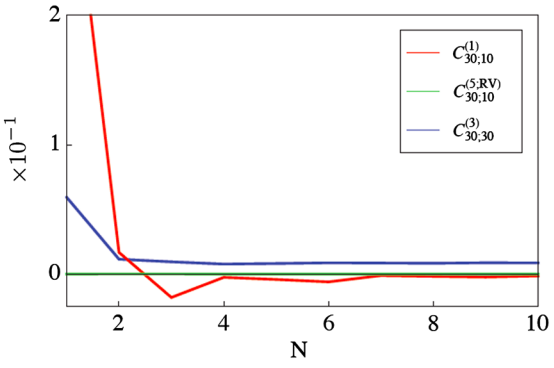

FIG. 3 (color online). A comparison between the tree-level coefficients $C^{(d)}_{30;L'0}$ to illustrate the relative rates of convergence to the continuum limit.

As in the case of the operator that conserves angular momentum in the continuum limit, the subleading correction (and in this case the first nonzero contribution) to the coefficient is suppressed by $1/N^2$. This can be shown to be the case for all the subleading contributions to the coefficients $C^{(d)}_{LM;L'M'}$ as follows. As is evident from Eq. (5), the integrals that are required in calculating deviations from the continuum values have the general form

$$I^{i_1\ldots i_k} \sim \frac{3}{4\pi}\frac{(Na)^k}{k!}\sum_{\mathbf{p}\neq 0}\int_0^1 dy y^{2+k} \times \int d\Omega_{\hat{y}} e^{i2\pi N\mathbf{p}\cdot\mathbf{y}}\hat{y}^{i_1}\hat{y}^{i_2}\ldots\hat{y}^{i_k}Y_{LM}(\Omega_{\hat{y}}), \quad (10)$$

which can be written as

$$I^{i_1\ldots i_k} \sim \frac{3}{4\pi}\frac{(Na)^k}{k!}\frac{1}{(i2\pi N)^k}\sum_{\mathbf{p}\neq 0}\frac{\partial}{\partial p_{i_1}}\cdots\frac{\partial}{\partial p_{i_k}} \times \int_0^1 dy y^{2+k}\int d\Omega_{\hat{y}} e^{i2\pi N\mathbf{p}\cdot\mathbf{y}} Y_{LM}(\Omega_{\hat{y}}) \sim \frac{3}{4\pi}\frac{(Na)^k}{k!}\frac{4\pi i^L}{(i2\pi N)^k}\sum_{\mathbf{p}\neq 0}\frac{\partial}{\partial p_{i_1}}\cdots\frac{\partial}{\partial p_{i_k}} Y_{LM}(\Omega_{\hat{p}}) \times \int_0^1 dy y^{2+k} j_L(2\pi N|\mathbf{p}|y). \quad (11)$$

The y integration over the Bessel function gives rise to either $-\frac{\cos(2\pi N|\mathbf{p}|)}{(2\pi N|\mathbf{p}|)^2}$ or $-\frac{\sin(2\pi N|\mathbf{p}|)}{(2\pi N|\mathbf{p}|)^2}$, up to higher orders in $1/N$, depending on whether L is even or odd. Thus the LO contribution from Eq. (11) in the large N limit is obtained by acting on the numerator with the p derivatives, producing k powers of N, multiplying the $1/N^2$ from the denominator. Therefore, Eq. (11) scales as

$$I^{i_1\ldots i_k} \sim (Na)^k\frac{1}{N^k}\frac{N^k}{N^2} \sim \frac{1}{\Lambda^k}\frac{1}{N^2}, \quad (12)$$

and, in general, the deviation of any coefficient from its continuum value is suppressed by $1/N^2 = \Lambda^2 a^2$. This result implies that in calculating the matrix element of $L = 3$ operator, one has a derivative expansion of the form

$$\Lambda^3\hat{\theta}_{3,0}(\mathbf{x};a,N) = \alpha_1\frac{\Lambda^2}{N^2}\mathcal{O}_z^{(1)}(\mathbf{x};a) + \alpha_2\frac{1}{N^2}\mathcal{O}_z^{(3)}(\mathbf{x};a) + \alpha_3\frac{1}{\Lambda^2N^2}\mathcal{O}_z^{(5)}(\mathbf{x};a) + \alpha_4\frac{1}{\Lambda^2N^2}\mathcal{O}_z^{(5;RV)}(\mathbf{x};a) + \alpha_5\mathcal{O}_{zzz}^{(3)}(\mathbf{x};a) + \alpha_6\frac{1}{\Lambda^2}\mathcal{O}_{zzz}^{(5)}(\mathbf{x};a) + \alpha_7\frac{1}{\Lambda^2N^2}\mathcal{O}_{zzzzz}^{(5)}(\mathbf{x};a) + \mathcal{O}\left(\frac{\nabla_z^7}{\Lambda^4}\right), \quad (13)$$

where the mixing with $L \neq 3$ operators (with coefficients $\alpha_{1,2,3,7,\ldots}$), as well as the operator with broken rotational symmetry (with coefficient α_4), vanish in the large N limit, while the coefficients of $L = 3$ operators (with coefficients $\alpha_{5,6,\ldots}$), are fixed by the scale of the operator, Λ. It is clear that for $N = 1$ and $\Lambda = 1/a$, where no smearing is performed, the problem with divergent coefficients of the lower dimensional operators is obvious, as, for example, the coefficient of $\mathcal{O}_z^{(1)}(\mathbf{x};a)$ diverges as $1/a^2$ as $a \to 0$, as is well known.

The fact that all the subleading contributions to the classical operator are suppressed at least by $1/N^2$ regardless of L and L' can be understood as follows. In the classical limit, where the short distance fluctuations of the operator are negligible, the operator does not probe the distances of the order of lattice spacing when $a \to 0$. The angular resolution of the operator is dictated by the solid angle discretization of the physical region over which the operator is smeared, and therefore is proportional to $1/N^2$. The question to answer is whether the quantum fluctuations modify this general result.

Before proceeding with the quantum loop calculations, it is advantageous to transform the operator into momentum-space to simplify loop integrals. This can be done easily by noting that for zero momentum insertion, the operator acting on the field with momentum $\mathbf{k}$ is

$$\hat{\tilde{\theta}}_{LM}(\mathbf{k};a,N) = \frac{3}{4\pi N^3}\sum_{\mathbf{n}}^{|\mathbf{n}|\leq N} e^{i\mathbf{k}\cdot\mathbf{n}a}Y_{LM}(\mathbf{n})\tilde{\phi}(\mathbf{k})\tilde{\phi}(-\mathbf{k}), \quad (14)$$

which, after using the partial-wave expansion of $e^{i\mathbf{k}\cdot\mathbf{n}a}$ and the exponential term resulting from the Poisson relation, can be written as

$$\hat{\tilde{\theta}}_{LM}(\mathbf{k};a,N) = 6\sqrt{\pi}\tilde{\phi}(\mathbf{k})\tilde{\phi}(-\mathbf{k})\sum_{\mathbf{p}}\sum_{L_1,M_1,L_2,M_2} i^{L_1+L_2}\sqrt{\frac{(2L_1+1)(2L_2+1)}{2L+1}}\langle L_1 0; L_2 0|L0\rangle \times \langle L_1M_1; L_2M_2|LM\rangle Y_{L_1M_1}(\Omega_{\hat{k}})Y_{L_2M_2}(\Omega_{\hat{p}})\int_0^1 dy y^2 j_{L_1}(aN|\mathbf{k}|y)j_{L_2}(2\pi N|\mathbf{p}|y). \quad (15)$$

Although this form seems to be somewhat more complicated than in position-space, it turns out that it is advantageous to work in momentum-space when dealing with higher angular momenta, as well as for $M \neq 0$. Further, the dimensionless parameters $|\mathbf{k}|/\Lambda$ and N that define the physics of such systems are now explicit. It is straightforward to show this form recovers the values of the leading and subleading coefficients given in Eqs. (8) and (9), and it is worth mentioning how they emerge from Eq. (15). For a nonzero value of $|\mathbf{p}|$ and $N = \infty$, the spherical Bessel function $j_{L_2}(2\pi N|\mathbf{p}|y)$ vanishes for any value of L_2. However, for large values of N but $|\mathbf{p}| = 0$ the only nonzero contribution is from $L_2 = 0$, and thus $L_1 = L$, leaving a straightforward integration over a single spherical Bessel function $j_L(aN|\mathbf{k}|y)$ to obtain the continuum limit given in Eq. (6). Extracting the subleading contributions and the violations of rotational symmetry is somewhat more involved, and we provide an explicit example in Appendix B.

B. Quantum corrections in $\lambda\phi^4$

In order to determine the impact of quantum fluctuations on the matrix elements of $\hat{\theta}_{L,M}$, defined in Eq. (1), we

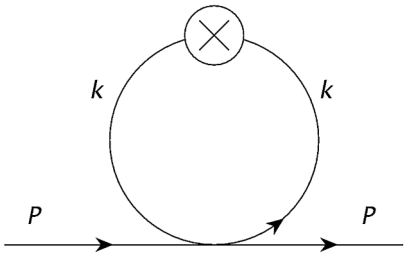

FIG. 4. One-loop correction to the two-point function with an insertion of $\hat{\theta}_{L,M}$ in $\lambda\phi^4$

consider loop contributions in $\lambda\phi^4$ theory. Beside its simplicity which enables us to develop tools in performing the analogous calculations in lattice QCD, this theory corresponds to some interesting condensed matter systems. For example, three dimensional O(N) models, which describe important critical phenomena in nature, have a corresponding $\lambda\phi^4$ field theory formulation. As pointed out in Refs. [48,49], anisotropy in space either due to the symmetries of the physical system, or due to an underlying lattice formulation, will result in the presence of irrelevant operators in the effective Hamiltonian which are not rotationally invariant, and introduce deviations of two-point functions from their rotationally invariant scaling law near the fixed point. However, as the rotationally invariant fixed point of the theory is approached, the anisotropic deviations vanish like $1/\xi^\rho$ where ξ^2 is the second moment correlation length derived from the two-point function, and ρ is a critical exponent which is related to the critical effective dimension of the leading irrelevant operator breaking rotational invariance. It has been shown that in the large N approximation of $O(N)$ models, $\rho \simeq 2$ for cubic-like lattices. In the following, it will be shown that, by inserting $\hat{\theta}_{L,M}$ defined in Eq. (1) into the two-point function, the same scaling law emerges when approaching the rotational-invariant continuum limit of $\lambda\phi^4$ theory.

At tree level, the contributions to the two-point function from an insertion of $\hat{\theta}_{L,M}$ at zero momentum transfer has been already discussed in Sec. II A. At one-loop, there is only one diagram with an insertion of $\hat{\theta}_{L,M}$ that contributes to the two-point function, as shown in Fig. 4. This diagram introduces corrections only to the $L = 0$ matrix element as there are no free indices associated with the loop. The lattice integral associated with this one-loop diagram is

$$J_{LM} = \frac{3\lambda}{4\pi N^3} \sum_{\mathbf{n}}^{|\mathbf{n}|\le N} \int_{-(\pi/a)}^{\pi/a} \frac{d^4k}{(2\pi)^4} \frac{e^{i\mathbf{k}\cdot\mathbf{n}a}}{(\hat{k}^2 + m^2)^2} Y_{LM}(\Omega_{\mathbf{n}}), \tag{16}$$

where $\hat{k}^2 = \frac{4}{a^2}\sum_\mu \sin^2(\frac{k_\mu a}{2})$, λ is the coupling constant and m is the ϕ mass. The three-momentum integration can be evaluated by noting that the region of integration can be split into two parts: region I where $0 \le |\mathbf{k}| \le \pi/a$ and therefore is rotationally symmetric, and region II where $\pi/a \le |\mathbf{k}| \le \sqrt{3}\pi/a$ which consists of disconnected angular parts. Also as the three-momentum integration is UV convergent, a small a expansion of the integrand can be performed. Using Eq. (15), the contribution from region I to the $\mathbf{p} = 0$ term in the Poisson sum is

$$\begin{aligned} J^{(I)}_{LM}(\mathbf{p} = 0) &= \frac{3\lambda}{(2\pi)^4} i^L \int_{-(\pi/a)}^{\pi/a} dk_4 \int_0^{\pi/a} dk k^2 \int d\Omega_{\hat{\mathbf{k}}} \frac{1}{(\hat{k}^2 + m^2)^2} \\ &\quad \times \left[\int_0^1 dy y^2 j_L(aN|\mathbf{k}|y)\right] Y_{LM}(\Omega_{\mathbf{k}}) \\ &= \frac{3\lambda}{16\pi^4} i^L [J^{\mathrm{LO}}_{LM} + J^{\mathrm{NLO}}_{LM} + \mathcal{O}(1/N^4)], \end{aligned} \tag{17}$$

where

$$\begin{aligned} J^{\mathrm{LO}}_{LM} &= 2\sqrt{\pi}\delta_{L,0}\delta_{M,0} \int_{-(\pi/\Lambda a)}^{\pi/\Lambda a} dq_4 \int_0^{\pi/\Lambda a} dq q^2 \frac{1}{[q^2 + q_4^2 + m^2/\Lambda^2]^2} \int_0^1 dy y^2 j_0(qy), \\ J^{\mathrm{NLO}}_{LM} &= \frac{1}{N^2} \int_{-(\pi/\Lambda a)}^{\pi/\Lambda a} dq_4 \int_0^{\pi/\Lambda a} dq q^2 \frac{q^4}{[q^2 + q_4^2 + m^2/\Lambda^2]^3} \left[\frac{6\sqrt{\pi}}{5}\delta_{L,0}\delta_{M,0} \int_0^1 dy y^2 j_0(qy)\right. \\ &\quad \left. + \delta_{L,4}\left(\frac{2}{3}\sqrt{\frac{2\pi}{35}}\delta_{M,-4} + \frac{4\sqrt{\pi}}{15}\delta_{M,0} + \frac{2}{3}\sqrt{\frac{2\pi}{35}}\delta_{M,4}\right) \int_0^1 dy y^2 j_4(qy)\right], \end{aligned} \tag{18}$$

with $q = |\mathbf{k}|/\Lambda$ and $q_4 = k_4/\Lambda$. The LO integral, J^{LO}_{LM}, is convergent, while the next-to-leading-order (NLO) contribution, J^{NLO}_{LM}, while not convergent, is not divergent, but is of the form $\sin(N\pi)/N^2$. This implies that they depend on the ratio of the two mass scales, Λ and m, but without inverse powers of a. So as $a \to 0$, the LO $L = 0$ operator makes an unsuppressed contribution to the $L = 0$ matrix element, while the contributions to this matrix element from the NLO rotational symmetry violating $L = 0$ and $L = 4$ operators are suppressed by $1/N^2$.

A simple argument shows that contributions from integration region II, for which $\pi/a \le |\mathbf{k}| \le \sqrt{3}\pi/a$, are also suppressed by $1/N^2$. After defining a new momentum variable $l_\mu = k_\mu a$ and $l^2 = l_1^2 + l_2^2 + l_3^2$, the $\mathbf{p} = 0$ term of the Poisson sum in region II is

$$J^{(II)}_{LM}(\mathbf{p}=0)=\frac{3\lambda}{16\pi^4}i^L\int_{-\pi}^{\pi}dl_4\int_{\pi}^{\sqrt{3}\pi}dll^2\int_{f(\Omega_{\mathbf{l}})}d\Omega_{\mathbf{l}} \times\frac{Y_{LM}(\Omega_{\mathbf{l}})}{(4\sum_\mu\sin^2(l_\mu/2)+a^2m^2)^2}\int_0^1 dyy^2 j_L(Nly), \tag{19}$$

where $f(\Omega_{\mathbf{l}})$ identifies the angular region of integration, and whose parametric form does not matter for this discussion. This region still exhibits cubic symmetry, and gives rise to contribution to the $L = 0, 4, 6, 8, \ldots$ operators. On the other hand, the three-momentum integration is entirely located in the UV as $a \to 0$, and thus

$$\sin^2(l_1/2) + \sin^2(l_2/2) + \sin^2(l_3/2) + \sin^2(l_4/2) \geq 1. \tag{20}$$

Also, integration over the Bessel function brings in a factor of $-\cos(Nl)/(N^2l^2)$, up to higher orders in $1/N$. So the integrand does not have any singularities in region II of the integration, and is bounded. As a result,

$$\left|J^{(II)}_{LM}(\mathbf{p}=0)\right| \leq\frac{1}{N^2}\frac{3\lambda}{(4\pi)^4}\int_{-\pi}^{\pi}dl_4\int_{\pi}^{\sqrt{3}\pi}dl\int_{f(\Omega_{\mathbf{l}})}d\Omega_{\mathbf{l}}Y_{LM}(\Omega_{\mathbf{l}}), \tag{21}$$

and consequently $J^{(II)}_{LM}(\mathbf{p} = 0)$ itself is suppressed by $1/N^2$. This completes the discussion of the $\mathbf{p} = 0$ term in the Poisson sum, corresponding to a zero-momentum insertion of the continuum operator into the loop diagram. It then remains to determine the scaling of the $\mathbf{p} \neq 0$ terms in the summation in the large N limit. The integral arising from the $\mathbf{p} \neq 0$ terms is, up to numerical factors,

$$\mathcal{I}_{\mathbf{p}\neq0} \sim \lambda\sum_{\mathbf{p}\neq0}\int_{-(\pi/a)}^{\pi/a}\frac{d^4k}{(2\pi)^4} \times\frac{1}{(\hat{k}^2+m^2)^2}Y_{L_1M_1}(\Omega_{\hat{k}})Y_{L_2M_2}(\Omega_{\hat{p}}) \times\int_0^1 dyy^2 j_{L_1}(Na|\mathbf{k}|y)j_{L_2}(2\pi N|\mathbf{p}|y). \tag{22}$$

This integral is finite in UV, and the integrand can be expanded in powers of a, giving a leading contribution of

$$\mathcal{I}_{\mathbf{p}\neq0} \sim \lambda\sum_{\mathbf{p}\neq0}\int_{-(\pi/\Lambda a)}^{\pi/\Lambda a}\frac{d^3qdq_4}{(2\pi)^4} \times\frac{1}{(q^2+q_4^2+m^2/\Lambda^2)^2}Y_{L_1M_1}(\Omega_{\hat{\mathbf{q}}})Y_{L_2M_2}(\Omega_{\hat{p}}) \times\int_0^1 dyy^2 j_{L_1}(qy)j_{L_2}(2\pi N|\mathbf{p}|y). \tag{23}$$

A nonzero angular integration requires that $L_1 = 0$, and the integral is suppressed at least by a factor of $1/N^2$ as integration over the Bessel functions introduces a factor of $1/(2\pi N|\mathbf{p}|)^2$ up to a numerical coefficient and a bounded trigonometric function at LO in $1/N$. The next order term in the small a expansion of the integrand can be easily shown to bring in an additional factor of $1/N^2$. So one can see that the $\mathbf{p} \neq 0$ terms in the Poisson summation, which give rise to noncontinuum contributions to the two-point function at one loop, are always suppressed by at least a factor of $1/N^2$.

The result of the one-loop calculation is promising: all the sub-leading contributions that break rotational symmetry are suppressed by $1/N^2$ compared to the leading $L = 0$ continuum operator contribution to the two-point function. A little investigation shows that this scaling also holds to higher orders in $\lambda\phi^4$ theory. Suppose that the operator is inserted into a propagator inside an n-loop diagram contributing to the two-point function. Considering the continuum part of the operator first, the leading term in the small a expansion of the integrand gives rise to $2n$ propagators, while the integration measure contributes $4n$ powers of momentum. Although this appears to be logarithmically divergent, the spherical Bessel function contributes a factor of inverse three-momentum and either a sine or cosine of the three-momentum, rendering the diagram finite. The same argument applies to the NLO term in the small a expansion of the integrand, resulting in a $1/N^2$ suppression of the breaking of rotational invariance. Insertion of the noncontinuum operator in loop diagrams are also suppressed by $1/N^2$ for similar reasons.

The interpretation of finite size scaling results presented in Refs. [48,49] in terms of what has been observed in this section is now straightforward. Near the critical point, the correlation length is the only relevant physical scale in the problem, and tends to infinity. So as the critical point is approached, one does not probe the underlying lattice structure as the correlation length becomes much larger than the lattice spacing, and extends over an increasing number of point shells. In comparison, inserting an operator which only probes distances of the order of a physical scale that is much larger than the lattice spacing, resembles the physics near a rotational-invariant fixed point, and the same scaling law for the nonrotational invariant operators is expected (in the same theory) as the lattice spacing goes to zero.

III. OPERATORS IN QCD

The necessity of introducing a gauge link to connect the fermionic fields in a gauge invariant way, makes the discussion of the operator and its renormalization more involved in gauge theories. The reason is two-folded: first, as is well known, perturbative LQCD is ill-behaved as a result of nonvanishing tadpoles which diverge in the UV, making the small coupling series expansion of the operators slowly convergent. The other difficulty is that as the operator is smeared over many lattice sites, the links are necessarily extended links. Thus, to analytically investigate the deviations from a rotational invariant path,

working with a well-defined path on the grid is crucial. In this section, the strategies to deal with these problems are discussed, and the scaling laws of different operator contributions to the two-point function in QCD with an insertion of the smeared operator are deduced.

In position-space, perhaps the simplest gauge-invariant smeared operator of quark bilinears is

$$\hat{\theta}_{L,M}(\mathbf{x}; a, N) = \frac{3}{4\pi N^3} \sum_{\mathbf{n}}^{|\mathbf{n}|\le N} \bar{\psi}(\mathbf{x}) U(\mathbf{x}, \mathbf{x}+\mathbf{n}a) \psi(\mathbf{x}+\mathbf{n}a) Y_{L,M}(\hat{\mathbf{n}}), \tag{24}$$

where

$$U(\mathbf{x}, \mathbf{x}+\mathbf{n}a) = e^{ig\int_{\mathbf{x}}^{\mathbf{x}+\mathbf{n}a} \mathbf{A}(z)\cdot d\mathbf{z}} = 1 + ig\int_{\mathbf{x}}^{\mathbf{x}+\mathbf{n}a} \mathbf{A}(z)\cdot d\mathbf{z} + \mathcal{O}(g^2), \tag{25}$$

where the actual path defining U will be considered subsequently. As the fermion operator is a spin singlet, $S = 0$, the total angular momentum of this operator in the continuum is $J = L$. One could also consider operators of the form

$$\hat{\theta}^{\mu}_{JL,M}(\mathbf{x}; a, N) = \frac{3}{4\pi N^3} \sum_{\mathbf{n}}^{|\mathbf{n}|\le N} \bar{\psi}(\mathbf{x}) \gamma^{\mu} U(\mathbf{x}, \mathbf{x}+\mathbf{n}a) \times \psi(\mathbf{x}+\mathbf{n}a) Y_{L,M}(\hat{\mathbf{n}}), \tag{26}$$

which can be used to form operators with $J = L+1$, L, $L-1$. It is clear that the set of operators with angular momentum J will mix under renormalization, but the vector nature of QCD precludes mixing between the $\bar{\psi}\psi$ and $\bar{\psi}\gamma^{\mu}\psi$ operators in the chiral limit. However to capture the main features of operator mixing in the continuum limit of LQCD, it suffices to work with the simplest operator, in Eq. (24). At tree level, the contributions of this operator away from the continuum limit scale in the same way as in the scalar theory, with contributions that violate rotational invariance suppressed by $\sim 1/N^2$.

Let us first discuss the one-loop renormalization of the operator in the continuum. There are four one-loop diagrams contributing to the operator renormalization as shown in Fig. 5. The diagram in Fig. 5(a) results from inserting the LO term in the small coupling expansion of the operator in the loop. At zero external momentum this diagram is

$$\Gamma^{(5a)} \sim -T^a T^a \frac{3ig^2}{4\pi} \int_0^1 dy y^2 \int d\Omega_{\mathbf{y}} \int \frac{d^4k}{(2\pi)^4} \times \frac{\gamma_{\alpha}(ik_{\mu}\gamma^{\mu} + m)^2 \gamma^{\alpha}}{(k^2+m^2)^2 k^2} e^{iNa\mathbf{k}\cdot\mathbf{y}} Y_{LM}(\Omega_{\mathbf{y}}), \tag{27}$$

which is clearly convergent in the UV. Also it contains $L = 0$ as well as $L = 1$ operator as can be seen from the angular part of the integral

$$\sum_{L',M'} \int d\Omega_{\mathbf{y}} d\Omega_{\mathbf{k}} [f_1(k^2, m, k_4) + f_2(k^2, m, k_4)\mathbf{k}\cdot\vec{\gamma}] \times Y_{L'M'}(\Omega_{\mathbf{k}}) Y^*_{L'M'}(\Omega_{\mathbf{y}}) Y_{LM}(\Omega_{\mathbf{y}}) = \sqrt{4\pi} f_1(k^2, k_4, m)\delta_{L,0}\delta_{M,0} + \sqrt{\frac{4\pi}{3}} f_2(k^2, k_4, m)|\mathbf{k}|\delta_{L,1}\Big[\gamma_1\Big(\frac{\delta_{M,-1} - \delta_{M,1}}{\sqrt{2}}\Big) + i\gamma_2\Big(\frac{\delta_{M,-1} + \delta_{M,1}}{\sqrt{2}}\Big) + \gamma_3\delta_{M,0}\Big], \tag{28}$$

where f_1 and f_2 are some functions of their arguments. One can check however that as $m/\Lambda \to 0$ (the chiral limit), the contribution to the $L = 1$ operator is suppressed by the quark mass.

The diagrams in Fig. 5(b) comes from the next term in the expansion of Eq. (25). It is straightforward to show that the Feynman rule for the one-gluon vertex with zero momentum insertion into the operator is

$$V_g^{\lambda} = \frac{3}{4\pi N^3} \sum_{\mathbf{n}}^{|\mathbf{n}|\le N} g a n^{\lambda} \frac{1}{(\mathbf{p}-\mathbf{p}')\cdot\mathbf{n}a} (e^{i(\mathbf{k}+\mathbf{p}')\cdot\mathbf{n}a} - e^{i\mathbf{p}'\cdot\mathbf{n}a}) \times \delta^4(p - p' - k) Y_{L,M}(\hat{\mathbf{n}}), \tag{29}$$

where the radial path between points $\mathbf{x}$ and $\mathbf{x}+\mathbf{n}a$ is taken in evaluating the link integral, p and p' are the momenta of incoming and outgoing fermions respectively, λ is the Lorentz-index of the gluon field, and k is the momentum of the gluon coming out of the vertex. Note that in principle, any path between points $\mathbf{x}$ and $\mathbf{x}+\mathbf{n}a$ can be taken in the above calculation, but if one is interested in deviations of the renormalized lattice operator from the rotational invariance compared to the continuum operator, a path between two points should be chosen in the continuum in

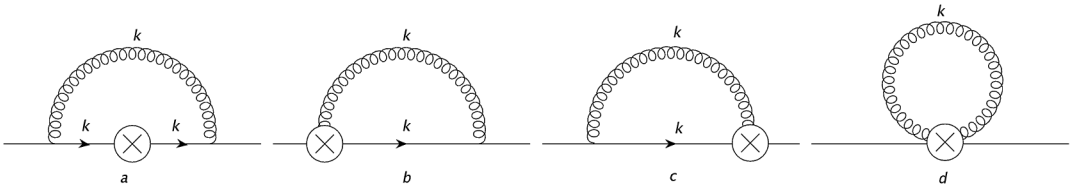

FIG. 5. One-loop QCD corrections to the fermionic two-point function with an insertion of $\hat{\theta}_{L,M}$, given in Eq. (24), at zero external momentum

such a way that it respects rotational invariance explicitly. Any path other than the radial path, on the other hand, is equivalent to infinitely many other paths resulting from rotated versions of the original path around the radial path. To reveal rotational invariance at the level of the continuum operator, an averaging over these infinite copies of the path is needed, and this makes the calculation of the link more involved.

Now at zero external momentum, using expression (29) with $p = 0$, the contribution from the second and third diagrams in Fig. 5(b) is

$$\Gamma^{(5b,5c)} \sim -T^a T^a \frac{3g^2}{2\pi} \int_0^1 dy y^2 \int d\Omega_{\mathbf{y}} \int \frac{d^4k}{(2\pi)^4} \times \frac{i\mathbf{k}\cdot\mathbf{y} + m\mathbf{y}\cdot\vec{\gamma}}{(k^2+m^2)k^2} \frac{1}{\mathbf{k}.\mathbf{y}} (e^{iNa\mathbf{k}\cdot\mathbf{y}} - 1) Y_{LM}(\Omega_{\mathbf{y}}). \quad (30)$$

As is evident, because of a nonoscillatory contribution to the operator, there is a logarithmically divergent piece from the above integration contributing to the $L = 0$ operator, which along with the logarithmic divergent contribution from wave function renormalization, contributes to the anomalous dimension of the operator. Also the angular integration of the above expression:

$$\int d\Omega_{\mathbf{y}} d\Omega_{\mathbf{k}} \left[1 + \frac{\mathbf{y}\cdot\vec{\gamma}}{i\mathbf{k}\cdot\mathbf{y}} m\right] (e^{iNa\mathbf{k}\cdot\mathbf{y}} - 1) Y_{LM}(\Omega_{\mathbf{y}}) = \int d\Omega_{\mathbf{y}} [g_1(Nay|\mathbf{k}|) + g_2(Nay|\mathbf{k}|) m\mathbf{y}\cdot\vec{\gamma}] Y_{LM}(\Omega_{\mathbf{y}}), \quad (31)$$

indicates that as before, in addition to $L = 0$ operator, an $L = 1$ contribution is present which is finite at UV, and can be shown to vanish for $m/\Lambda \to 0$. g_1 and g_2 are some functions of their arguments whose explicit forms do not matter for this discussion.

The last diagram in Fig. 5 corresponds to the $\mathcal{O}(g^2)$ term in the small coupling expansion of the gauge link. It contains the tadpole of the continuum theory whose value depends in general on the regularization scheme. For example, by using a hard momentum cutoff which is matched easily with the lattice regularization, it diverges quadratically. However, it is not hard to see that in dimensional regularization which respects the full rotational symmetry of the continuum, it vanishes in $d = 4$, therefore it does not contribute to the renormalization of the continuum operator. But the fourth diagram in Fig. 5 does not only include the conventional tadpoles, Fig. 6(a), it also contains the diagram where a gluon is emitted by the Wilson line inside the operator and then absorbed at another point on the Wilson line, Fig. 6(b) as a consequence of the matter fields being separated by a distance $\mathbf{n}a$. It is straightforward to show this diagram is convergent, and scales by $\alpha_s/|\mathbf{\Delta x}|^2$ where $\mathbf{\Delta x}$ is the distance between two gluon vertices and α_s is evaluated at the energy scale of the order of $1/|\mathbf{\Delta x}|$. This completes the qualitative discussion of the operator renormalization and mixing at one-loop order in the continuum.

Let us start the discussion of the lattice operator by assuming that its definition is still given by Eq. (24). However, this can be shown to be a naive definition of the operator on the lattice. The reason is implicit in the discussion of tadpoles given above. Although tadpoles are absent from the operator renormalization in the continuum, on the lattice, they are nonvanishing, and result in large renormalizations, as can be seen in perturbative lattice QCD calculations. As was suggested long ago by Lepage and Mackenzie [50], to make the perturbative expansion of the lattice quantities well behaved, and to define an appropriate connection between the lattice operators and their continuum counterparts, one can remove tadpoles from the expansion of the lattice operators in a nonperturbative manner by dividing the gauge link by its expectation value in a smooth gauge,

$$U(x, x + a\hat{\mu}) \to \frac{1}{u_0} U(x, x + a\hat{\mu}), \quad (32)$$

where a simpler, gauge invariant choice of u_0 uses the measured value of the plaquette in the simulation, $u_0 \equiv \langle \frac{1}{3} \mathrm{Tr}(U_{\mathrm{plaq}}) \rangle^{1/4}$. There remains still another issue regarding the tadpole contributions to the smeared operator which is not fully taken care of by the simple single-link improvement procedure explained above. The operator introduced in Eq. (24) is smeared over several lattice sites, and as a result includes extended links. As will be explained shortly, in spite of $\mathcal{O}(\alpha_s)$ corrections due to tadpoles from a single link, there is an $\mathcal{O}(N\alpha_s)$

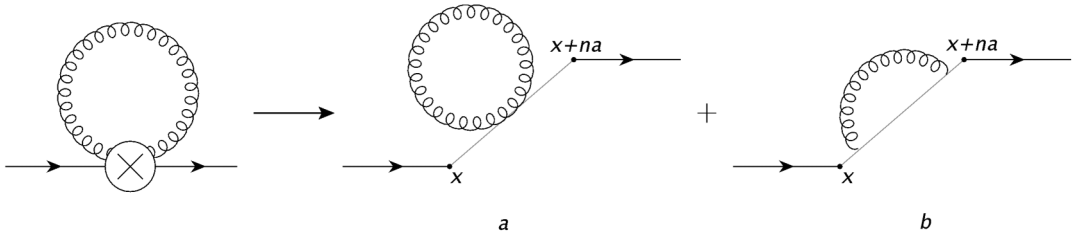

FIG. 6. The tadpole contribution consists of the conventional tadpole diagram (a), which vanishes when using a mass-independent regulator in the continuum (such as dimensional regularization), as well as the diagram shown in (b) which is of the order of $\alpha_s/|\mathbf{\Delta}x|^2$, where $\mathbf{\Delta x}$ is the distance between two gluon vertices.

enhancement due to the tadpoles from the extended link with length $\sim Na$. So although a nonperturbative tadpole improvement could introduce nonnegligible statistical errors, this improvement is crucial, otherwise the relation between the lattice smeared operator and the corresponding continuum operator is somewhat obscure.

The reason for the $\mathcal{O}(N\alpha_s)$ enhancement of tadpoles from the extended links can be illustrated by working out a particular example. Suppose that the link is extended between points $\mathbf{x}$ and $\mathbf{x} + Na\hat{e}_1$ entirely along the $\mathbf{1}$ axis. Then in order to make a tadpole, not only can each gauge field be contracted with the other gauge field belonging to the same elementary link, but also it can be contracted with a gauge field from one of the remaining $N-1$ elementary links (see Fig. 7). Note that each diagram in Fig. 7 comes with a multiplicity of $N-m$, where m is the number of links between the contracted gluonic vertices. At LO in a, the corresponding contribution from the extended tadpole is of the form

$$\Gamma^{(\mathrm{ET})} \sim \alpha_s a^2 \int_{-(\pi/a)}^{\pi/a} d^4k \frac{e^{imak_1}}{k_1^2 + k_2^2 + k_3^2 + k_4^2} \sim \frac{\alpha_s}{m^2}, \tag{33}$$

from which the contribution from all the diagrams in Fig. 7 can be obtained,

$$\sum_{m=1}^{N-1} (N-m)\frac{\alpha_s}{m^2} = \mathcal{O}(N\alpha_s). \tag{34}$$

Note that the $m = 0$ term, corresponding to the first diagram in Fig. 7, has been excluded from the above sum as it is just the single link tadpole contribution. Given that there are N single links, the total contribution from single link tadpoles is $\mathcal{O}(N\alpha_s)$ as well.

Another issue with the extended links is the fact that without tadpole improvement, breakdown of rotational symmetry occurs at $\mathcal{O}(N\alpha_s)$. The reason is that without tadpole improvement of the extended links, contributions from the different A_1 irreps in a given point shell are normalized differently. For example, there are more tadpole diagrams at $\mathcal{O}(g^2)$ contributing to an extended link between points (0, 0, 0) and (2, 2, 1) (five single links) than to an extended link between points (0, 0, 0) and (3, 0, 0) (three single links) although both points belong to the same point shell (i.e., have the same separation in position-space). This fact magnifies the necessity of tadpole improvement as well as providing a prescription for an appropriate improvement of an extended link. As the expectation value of a link belonging to a given A_1 irrep in a given shell is in general different from the expectation value of the link belonging to another A_1 irrep in the same shell, one needs to redefine the link in a given irrep by dividing it by its expectation value in the same irrep,

$$U_{A_1^i}(x, x + a\mathbf{n}) \to \frac{1}{u_{A_1^i}} U_{A_1^i}(x, x + a\mathbf{n}), \tag{35}$$

where $u_{A_1^i} = \langle U_{A_1^i}(x, x + a\mathbf{n})\rangle$, and the A_1^i's are different A_1 irreps belonging to the n^2-shell. With this prescription for tadpole improvement of the extended links, the renormalized operator is assured to be safe from large rotational invariance breaking effects of the order of $\mathcal{O}(N\alpha_s)$. With this new definition of the gauge link, Eq. (24) is now a well-defined lattice operator with an appropriate continuum limit which can be used in our subsequent analysis.

As the cancellation of the tadpole diagram is assured by the new definition of the operator, there are only three one-loop diagrams that contribute to the renormalization of the lattice operator. The first diagram in Fig. 5 corresponds to the following loop integral at zero external momentum for Wilson fermions,

$$\begin{aligned}\Gamma^{(5a)} \sim\ & (ig)^2 T^a T^a \frac{3}{4\pi N^3} \sum_{\mathbf{n}} \int_{-(\pi/a)}^{\pi/a} \frac{d^4k}{(2\pi)^4} \\ & \times e^{i\mathbf{k}\cdot\mathbf{n}a}\left[\gamma_\rho \cos\left(\frac{k_\rho a}{2}\right) - ir\sin\left(\frac{k_\rho a}{2}\right)\right] \\ & \times \left(\frac{-i\sum_\mu \gamma_\mu \frac{\sin(k_\mu a)}{a} + M(k)}{\sum_\mu \frac{\sin^2(k_\mu a)}{a^2} + M(k)^2}\right)^2 \\ & \times \left[\gamma^\rho \cos\left(\frac{k^\rho a}{2}\right) - ir\sin\left(\frac{k^\rho a}{2}\right)\right] \\ & \times \frac{i}{\frac{4}{a^2}\sum_\nu \sin^2\left(\frac{k_\nu a}{2}\right)} Y_{LM}(\Omega_{\mathbf{n}}),\end{aligned} \tag{36}$$

where $M(k) \equiv M + 2r/a\sum_\mu \sin^2(k_\mu a/2)$, and r is the Wilson parameter. Clearly at LO in the lattice spacing, one recovers the corresponding diagram with the insertion of the continuum operator, Eq. (27), and so it contributes to both the $L = 0$ and $L = 1$ operators. Note that although the integration region is not rotationally symmetric like the continuum integral, the convergence of integral at UV

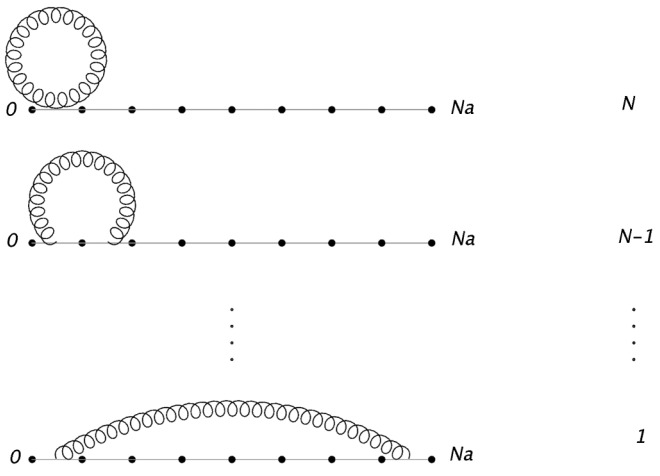

FIG. 7. Tadpole diagrams contributing to the smeared operator at one-loop order. Shown in the right are the number of diagrams of each type.

ensures that the contributions from nonrotationally symmetric integration region II, defined in Sec. II B, are suppressed by additional powers of $1/N$ compared to the rotational invariant region I:

$$\delta\Gamma^{(5a)} \sim -ig^2T^aT^a\frac{3i^L}{16\pi^4}\int_{-\pi}^{\pi}dl_4\int_{\pi}^{\sqrt{3}\pi}dll^2\int_{f(\Omega_1)}d\Omega_1 \times\frac{(il_\mu\gamma^\mu+ma)^2}{(l^2+m^2a^2)^2l^2}Y_{LM}(\Omega_1)\Big[\int_0^1 dyy^2j_L(Nly)\Big], \tag{37}$$

where: $l_\mu = k_\mu a$ and $l^2 = l_1^2 + l_2^2 + l_3^2$. The integrand is clearly convergent, and the integration region is entirely in the UV, and so the only dependence on $a = 1/(\Lambda N)$ comes from the integration over the Bessel function, giving a LO contribution proportional to $1/N^2$. However, the first subleading contribution from this diagram scales as $\sim\alpha_s/N$ for Wilson fermions instead of $\sim\alpha_s/N^2$. The reason is that the small a expansion of the integrand in Eq. (36) includes terms at $\mathcal{O}(a)$ which is proportional to the Wilson parameter. The integrand scales as $\sim 1/k^3$ multiplied by the spherical Bessel function in the UV which still gives rise to a convergent four-momentum integration for any value of L,

$$\delta\Gamma^{(5a,r)} \sim a\int d^4k\frac{1}{k^3}\Big[\int_0^1 dyy^2j_L(Naky)\Big] \sim a\Lambda = \frac{1}{N}. \tag{38}$$

These contributions are rotational invariant, and will be included in the renormalization Z-factor of the operator when matching the lattice operator with its continuum counterpart. Further, the integrals that appear at $\mathcal{O}(a^2)$ in an expansion of Eq. (36) are also convergent, and the terms containing rotational invariance breaking contributions are suppressed by $1/N^2$. This completes discussion of the first one-loop diagram of Fig. 5.

The second diagram contains the one-gluon vertex operator, and requires evaluating a line integral over the path on the grid defining the extended link. As was pointed out in the discussion of the path in the continuum, in general any path can be chosen in evaluating the operator both in the continuum or on the lattice, but requiring the recovery of rotational symmetry at the level of the operator means that the extended link has to exhibit rotational symmetry in the continuum limit. As already discussed, the simplest rotational invariant path in the continuum is the radial path between the points, so it makes sense to try to construct a path on the grid which remains as close as possible to the radial path between points x and $x + \mathbf{n}a$ as it passes through the lattice sites. One might expect though that choosing a path in continuum which is the same as its lattice counterpart is a more legitimate choice. One example of such a path is an L-shaped path. However, it is not hard to verify that the L-shaped link does not restore rotational invariance in the continuum limit as the continuum path explicitly breaks rotational symmetry. So the problem of evaluating the one-gluon vertex of the smeared operator is reduced to finding the closest path to the straight line on the grid. In a lattice calculation, one can, in principle, construct an algorithm which finds a path on the three-dimensional grid in such a way that the area between the path and the rotational invariant radial path is a minimum. One such algorithm has already been used in Ref. [32] to construct a path that follows the straight line between sites A and B as closely as possible, by forming a diagonal link at each step which has the maximum projection onto the vector $\vec{AB}$. By this construction of "super-links", the authors have been able to form arbitrary (approximate) rotations of the Wilson loops, therefore constructing glueball operators which project onto a definite spin J in the continuum limit. However, the analytic form of the super-link has not been given. In Appendix D, a method to evaluate the link on such a path is illustrated with a small number of examples. For the following discussion, however, a particular example has been considered which encapsulates the essential features of the recovery of the rotational invariant path, and gives us an idea how to deal with the general case.

Suppose that the link connects points x and $x + \mathbf{n}a$ on a cubic lattice where $\mathbf{n} = \frac{a_0}{a}(Q, 1, 0)$, and $a_0 = 2^K a$. As usual a denotes the lattice spacing, and Q is an arbitrary integer. The continuum limit is recovered when the integer K tends to infinity for a finite value of a_0. Then as is shown in Appendix D, for a path which is symmetric under reflection about its midpoint and remains as close as possible to the vector $\mathbf{n}a$ (see Fig. 8), the $\mathcal{O}(g)$ term in the momentum-space expansion of the link has the following form

$$U^{(1g)}(q) = ig\frac{a_0}{2^K}e^{i\mathbf{q}\cdot\mathbf{n}a/2}\frac{\sin\left(\frac{\mathbf{q}\cdot\mathbf{n}a}{2}\right)}{\sin\left(\frac{\mathbf{q}\cdot\mathbf{n}a}{2^{K+1}}\right)}\Big[A_y(q) + 2A_x(q) \times\frac{\sin(Qq_xa_0/2^{K+2})}{\sin(q_xa_0/2^{K+1})}\cos\left(\frac{Qq_xa_0}{2^{K+2}}+\frac{q_ya_0}{2^{K+1}}\right)\Big]. \tag{39}$$

As $K \to \infty$ limit which corresponds to $a \to 0$, one obtains

$$U^{(1g)}(q) = 2ige^{i\mathbf{q}\cdot\mathbf{n}a/2}\frac{\sin(\frac{\mathbf{q}\cdot\mathbf{n}a}{2})}{\mathbf{q}\cdot\mathbf{n}a}\Big[\mathbf{A}\cdot\mathbf{n}a + \frac{a^2}{24}(q_xQ+q_y)^2\mathbf{A}\cdot\mathbf{n}a - \frac{a^2}{24}QA_xa_0(q_x^2(Q^2-1)+3Qq_xq_y+3q_y^2) + \mathcal{O}(a^4)\Big], \tag{40}$$

recovering the continuum link, given in Eq. (29), and contains broken rotational invariance contributions which are suppressed by $\sim\mathcal{O}(a^2)$. This scaling has been shown in

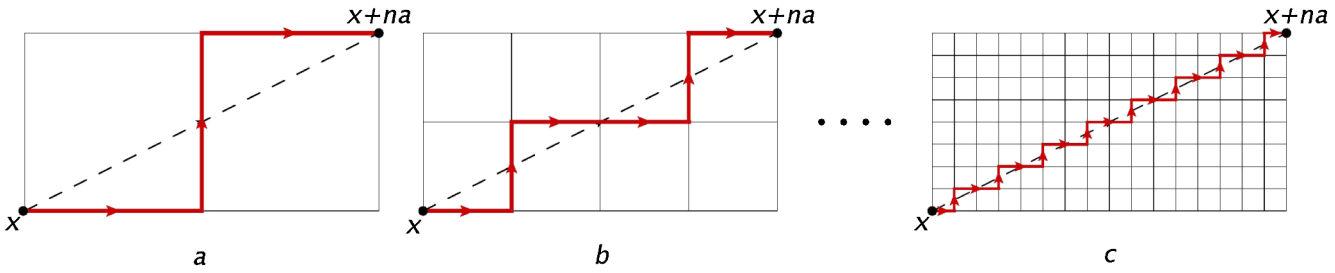

FIG. 8 (color online). (a) The link between points x and $x + \mathbf{n}a$ for $\mathbf{n} = (2, 1, 0)$ which remains as close as possible to the diagonal link. (b) The link between the same points for $\mathbf{n} = 2(2, 1, 0)$ which consists of two separate links of part (a) with the lattice spacing being halved. (c) The link for $\mathbf{n} = 2^K(2, 1, 0)$ which consists of 2^K separate links of part (a) with the lattice spacing divided by 2^K.

Appendix D to hold for vectors $\mathbf{n}$ of the forms: $\frac{a_0}{a}(Q, 1, 1)$, $\frac{a_0}{a}(Q, Q, 1)$, and $\frac{a_0}{a}(Q, Q, Q)$ as well.

Let us now examine how the insertion of this contribution from the operator modifies the scaling of the rotational invariance violating operators at one-loop. The contribution from the second diagram in Fig. 5 with the insertion of this vertex can be calculated order by order in small a by expanding the vertices and propagators as before. At the LO one gets

$$\Gamma^{(5b)} \sim -ig^2 T^a T^a \frac{3}{4\pi N^3} \sum_{\mathbf{n}} \int_{-(\pi/a)}^{\pi/a} \frac{d^4k}{(2\pi)^4} \frac{ik_\mu \gamma^\mu + m}{(k^2 + m^2)k^2} \times \frac{e^{i\mathbf{k}\cdot\mathbf{n}a} - 1}{i\mathbf{k}\cdot\mathbf{n}a} Y_{LM}(\Omega_{\mathbf{n}}) \Big[a\mathbf{n}\cdot\vec{\gamma} + \frac{a^2}{24}(k_x Q + k_y)^2 a\mathbf{n}\cdot\vec{\gamma} - \frac{a^2}{24} Q(k_x^2(Q^2 - 1) + 3Qk_x k_y + 3k_y^2)\gamma_x a_0 \Big]. \quad (41)$$

Clearly, after adding the contribution from the third diagram in Fig. 5, the LO contribution from the above expression, the first term in the bracket of Eq. (41), recovers the results obtained previously for the insertion of the continuum operator, up to suppressed contributions from the integration region II, as discussed before. Therefore this term contributes to the $L = 0$ operator with a logarithmically divergent coefficient, which along with the wave function renormalization contributes to the anomalous dimension of the lattice operator. Note that the wave function renormalization gives rise to a logarithmically divergent contribution to the $L = 0$ operator at LO in the lattice spacing, recovering the continuum result, and the subleading contributions are suppressed at least by $a = 1/(N\Lambda)$ for Wilson fermions. This term also contains and $L = 1$ operator which is proportional to m, and vanishes in the chiral limit.

The second term in the bracket of Eq. (41) is $\mathcal{O}(a^2)$, and can be written as

$$\delta\Gamma^{(5b,5c),2} = -i \frac{g^2 a^2}{8\pi N^3} T^a T^a \sum_{\mathbf{n}} \int_{-(\pi/a)}^{\pi/a} \frac{d^4k}{(2\pi)^4} \times \Big[1 + \frac{m}{i\mathbf{k}\cdot\mathbf{n}a} a\mathbf{n}\cdot\vec{\gamma} \Big] \frac{e^{i\mathbf{k}\cdot\mathbf{n}a} - 1}{(k^2 + m^2)k^2} \times (k_x Q + k_y)^2 Y_{LM}(\Omega_{\mathbf{n}}) \sim \mathcal{O}(g^2 a^0). \quad (42)$$

This scaling arises as a result of the UV divergence of the nonoscillatory contribution to the integral and is entirely a UV effect. For this term there is no dependence upon $\mathbf{n}$ and as such the factor of N^{-3} is canceled by a corresponding N^3 from the sum. Terms proportional to the mass are convergent in the UV, and as such are suppressed by a^2 in the continuum limit.

The last term in the above expression Eq. (41) contains rotational breaking contributions. It is multiplied by an explicit factor of a^2, but as seen in the previous term, the power divergence of the nonoscillatory part of the integral gives rise to an overall scaling of $\mathcal{O}(g^2)$. This completes the discussion of the one-loop corrections to the lattice operator for the specific displacement vector $\mathbf{n}a$ used above. It is also straightforward to check the obtained scaling of different terms for other choices of the vector $\mathbf{n}a$. In general, subleading contributions to the continuum link are $\mathcal{O}(a^2)$, and so by dimensional analysis it has an associated factor of momentum squared. On the other hand, it always contains a nonoscillatory term, and as a result, the noncontinuum contributions and the violations of rotational symmetry scale as $\mathcal{O}(\alpha_s)$.

Given the discussion of the previous paragraphs, we naively conclude that the rotational symmetry breaking scales as $\sim\mathcal{O}(\alpha_s)$ in the continuum limit. It is the one-gluon vertex associated with the smeared-operator that is dominating this behavior, with the contributions from other diagrams scaling as $\sim\alpha_s/N$ for Wilson fermions [Eqs. (36) and (37)] and α_s/N^2 from the other loop diagrams compared with $\sim 1/N^2$ from the tree-level matching. However, this scaling can be further improved by smearing the gauge-field. The $\mathcal{O}(\alpha_s)$ contributions are due to the explicit factor of a^2 being compensated by a quadratic loop divergence, $(\pi/a)^2$, rendering a suppression by only the coupling in the continuum limit, analogous to the impact of tadpole diagrams. However, by smearing the gluon field over a volume of radius $1/\Lambda_g = aN_g$,[3] the offending diagrams in Fig. 5 scale as

[3]We have distinguished the smearing radius of the operator, N, from the smearing radius of the gluons, N_g, but in principle they could be set equal.

$$\delta\Gamma^{(5b,5c),2,3} \sim \alpha_s a^2 \Lambda_g^2 \sim \frac{\alpha_s}{N_g^2}, \tag{43}$$

due to the suppression of the high momentum modes in the gluon propagator.

The natural question to ask here is what is the scale of the coupling in this process? Note that the bare coupling constant of lattice QCD suffers from large renormalization as discussed before, so a better-behaved weak coupling expansion of the lattice quantities uses a renormalized coupling constant as the expansion parameter. As is suggested by Lepage and Mackenzie [50], one first fixes the renormalization scheme by determining the renormalized coupling $\alpha_s^{\rm ren}(k^*)$ from a physical quantity such as the heavy quark potential. Then the scale of the coupling is set by the typical momentum of the gluon in a given process. In the case considered above, the energy scale of the strong coupling constant is dictated by the scale of the gluon smearing region as the dominant contribution to the integral comes from this region of the integration: $k^* \sim \pi/(N_g a)$. A better estimate of the scale can be obtained by the method explained in Ref. [50], but since we are interested in the continuum limit where $a \to 0$, this is already a reliable estimation of the momentum scale of the running coupling.

The analysis in QCD is more complex at one-loop level than in the scalar theory due to the presence of the gauge-link required to render the operator gauge-invariant. We have found that the contributions from the operator defined in Eq. (24) scale in the same way as those in the scalar theory, with the violation of rotational symmetry suppressed by factors of $\sim 1/N^2$, but both tadpole improvement of the extended links and smearing of the gauge-field is required. Our analysis of Wilson fermions reveals the contributions to matrix elements that violate rotational invariance in the continuum limit at the one-loop level are suppressed by factors of $\sim \alpha_s/N^2$ and $\sim \alpha_s/N_g^2$, and thus for a smearing defined in physical units, deviations from rotational invariance scale as $\mathcal{O}(a^2)$. Contributions that scale as $\sim \alpha_s/N$ and are proportional to the Wilson parameter, conserve angular momentum and can be absorbed by the operator Z-factor. Most importantly, as in the scalar theory, there are no mixings with lower dimension operators that diverge as inverse powers of the lattice spacing.

IV. SUMMARY AND CONCLUSIONS

In this paper, a mechanism for the restoration of rotational symmetry in the continuum limit of lattice field theories is considered. The essence of this approach is to construct an appropriate operator on the cubic lattice which has maximum overlap onto the states with definite angular momentum in the continuum. In analogy to the operator smearing proposals given in Refs. [24–26,32,33], the operator is constructed on multiple lattice sites. Using spherical harmonics in the definition of the operator is key to having the leading contributions to the classical operator be those with the desired angular momentum. The sizes of the contributions are controlled by the scale of the smearing of the operator, with sub-leading contributions to both lower and higher dimensional operators that violate rotational symmetry being suppressed by $1/N^2$—reflective of the pixelation of the operator and fields. The $\lambda\phi^4$ scalar field theory is shown to preserve this universal scaling of the leading non-rotationally invariant contributions at all orders in perturbation theory, compatible with the finite size scaling results of $\lambda\phi^4$-type theories near their rotational invariant fixed points [48,49]. The same can be shown to be true in $g\phi^3$ scalar field theory.

Gauge invariance somewhat complicates the construction and analysis of analogous operators in QCD. Although the tree-level lattice operator in QCD exhibits the same scaling properties as the scalar operator, extended gauge-links connecting the quark fields generate gluonic interactions that contribute to loop diagrams that are power-law divergent. Such contributions are either eliminated by tadpole improvement of the extended links, or are suppressed by smearing of the gauge-field. We find that it is the physical length-scales and continuum renormalization-scale that dictate the size of matrix elements. The leading noncontinuum corrections from the one-loop diagrams preserve angular momentum, scaling as $\sim \alpha_s a$ for Wilson fermions, and can be absorbed by the operator Z-factor. In contrast, contributions that violate rotational symmetry are suppressed by $\alpha_s a^2$ as $a \to 0$. While we have chosen a specific form for the smeared operator, we expect that the results, in particular the scaling of the violations to rotational symmetry, are general features of a smeared operator with any (smooth) profile. Also, it is worth mentioning that although the calculations preformed in this work, and the subsequent conclusions, relate operators and matrix elements in H(3) to those in O(3), the methodology and results are expected to hold in relations between H(4) and O(4). Instead of working with operators formed with spherical harmonics to recover SO(3) invariance, one would work with operators formed with hyper-spherical harmonics to recover O(4) symmetry.

We conclude the paper by discussing the practicality of our result for the current LQCD calculations as well as its connection to the infra-red (IR) rotational invariance recovery of the lattice theories:

(i) It is important to understand and to quantify the violation of angular momentum conservation in the states and matrix elements calculated using lattice QCD with the lattice spacings currently employed. One interesting result is that by using the tadpole-improved operator extended over several lattice sites and built from the smeared gauge links, the quantum corrections introduce noncontinuum corrections to the tree-level results that are suppressed by at least α_s, i.e., they do not introduce power-divergent contributions. As an example, suppose that a lattice

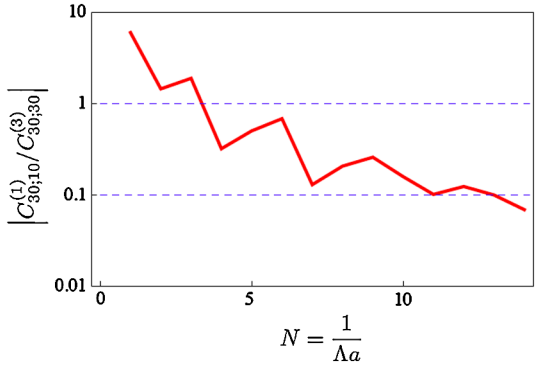

FIG. 9 (color online). The absolute value of the ratio of the tree-level coefficient, $C^{(1)}_{30;10}$, of a lowest dimension operator with $L = 1$ to the tree-level coefficient, $C^{(3)}_{30;30}$, of the lowest dimension operator with angular momentum, $L = 3$, resulting from the $L = 3$ operator in Eq. (1), as a function of the number of included point-shells.

calculation aims to determine a matrix element of an operator with $L = 3$. Then, as is demonstrated in Fig. 9, the coefficient of the lower dimensional derivative operator with $L = 1$ is almost 10 times larger than the coefficient of the $L = 3$ derivative operator when the operator is defined over one lattice site, $N = 1$. The computational time required to accurately perform the subtraction of the $L = 1$ contribution is significant for a smearing scale of, say, $\Lambda \sim 2$ GeV. Fortunately, by halving the lattice spacing and smearing the operator over just two point shells ($N = 2$), the contamination from the lower dimensional operator is reduced by a factor of $\sim$3, requiring a factor of $\sim$10 less computational resources to accurately perform the subtraction at the same level of precision. Further, by smearing the operator over ten point shells, the contamination from the lower dimensional operator is reduced to $\sim$1% of its value at $N = 1$. Given that the lattice spacing associated with $\Lambda = 2$ GeV is $a \sim 0.1$ fm for $N = 1$, to be able to smear out to the $N = 2$ shell requires a lattice spacing of $a \sim 0.05$ fm, pushing the limits of current lattice generation. To smear out to the $N = 10$ shell would require a lattice spacing of $a \sim 0.01$ fm which is currently impractical.

(ii) The restoration of rotational invariance as discussed in this paper regards only the UV asymptote of the lattice theories: as one reaches a good pixelation of a region of space where the lattice operator probes, the identification of eigenstates of the angular momentum operator becomes possible. In other words, the more point-shells included in the lattice operator, the larger overlap the operator has onto a definite angular momentum state. However, the full recovery of rotational invariance in the lattice theories requires the suppression of rotational symmetry breaking contributions to the physical quantities not only as a result of short-distance discretization effects, but also as a result of boundary effects of the finite cubic lattice in the IR regime of the theories. The finite size of the lattice imposes (anti-)periodic boundary conditions on the lattice wave functions which enforces the lattice momenta to be discretized, $\mathbf{p} = \frac{2\pi \mathbf{n}}{L}$, where L is the spatial extent of the lattice and $\mathbf{n}$ is a vector of integers. The IR rotational invariant theory is achieved as the lattice becomes infinitely large, corresponding to a large number of point-shells in the momentum-space. However, beyond this intuitive picture, one needs to examine in a quantitative way how this recovery takes place in the large volume limits of the lattice theories in the same way as it was discussed for small lattice spacing limit of the theories. One quantitative explanation of this IR recovery, has been given recently in Ref. [51] in the context of the extraction of phase shifts in higher partial-waves from the energies of scattering particles in a finite volume using Lüscher's method. The idea is that as one includes higher momentum shells, the number of occurrence (multiplicity) of any given irrep of the cubic group increases. As a result, for a fixed energy in the large volume limit, linear combinations of different states of a given irrep can be formed which can be shown to be energy eigenstates; and the energy-shift of each combination due to interactions is suppressed in all but one partial-wave in the infinite-volume limit. So, although each irrep state has an overlap onto infinitely many angular momentum states, the high multiplicity of a given irrep in a large momentum shell generates energy-eigenstates which dominantly overlap onto states of definite angular momentum, and the mixing with other angular momentum states becomes insignificant in the large volume limit. This picture also helps to better understand the mechanism of the UV rotational invariance recovery due to the operator smearing. It is the high multiplicity of the irreps in large (position-space) shells that is responsible for projecting out a definite angular momentum eigenstate. These large shells are obtained by reducing the pixelation of the lattice by taking $a \to 0$ in position-space, or increasing the size of the lattice by taking $L \to \infty$ in momentum-space—both are required in order to recover rotational invariance from calculations performed on a lattice.

ACKNOWLEDGMENTS

We would like to thank David B. Kaplan and Sichun Sun for their contributions to a precursor to this work, Saul Cohen, David B. Kaplan, Kostas Orginos, Stephen R. Sharpe, and Boris Spivak for useful discussions, and David B. Kaplan and Thomas C. Luu for their feedback

on the earlier draft of this paper. Z. D. and M. J. S. were supported in part by the DOE Grant No. DE-FG03-97ER4014.

APPENDIX A: OPERATOR BASIS

In this appendix, a basis for composite local operators is presented. Any local operator that is bilinear in the scalar field with L spatial indices, and that is invariant under cubic transformations, can be written as

$$\mathcal{O}^{(d)}_{i_1 i_2 \ldots i_L}(\mathbf{x}) = \phi^\dagger(\mathbf{x}) Q^{(d)}_{i_1 i_2 \ldots i_L} \phi(\mathbf{x}), \tag{A1}$$

where $Q^{(d)}_{i_1 i_2 \ldots i_L}$ is a homogeneous function of the operator ∇_i, and degree d ($d \geq L$) is defined to be the number of ∇'s. Their forms are determined by the symmetric traceless tensor of rank L that respect cubic symmetry constructed from d ∇'s. The operators composed of fewer than seven derivatives and with no spatial indices are

$$\begin{aligned}
\mathcal{O}^{(0)}(\mathbf{x}) &= \phi^\dagger(\mathbf{x})\phi(\mathbf{x}) \\
\mathcal{O}^{(2)}(\mathbf{x}) &= \phi^\dagger(\mathbf{x})\nabla^2\phi(\mathbf{x}) \\
\mathcal{O}^{(4)}(\mathbf{x}) &= \phi^\dagger(\mathbf{x})(\nabla^2)^2\phi(\mathbf{x}) \\
\mathcal{O}^{(4,RV)}(\mathbf{x}) &= \phi^\dagger(\mathbf{x})\sum_j \nabla_j^4\phi(\mathbf{x}) \\
\mathcal{O}^{(6)}(\mathbf{x}) &= \phi^\dagger(\mathbf{x})(\nabla^2)^3\phi(\mathbf{x}) \\
\mathcal{O}^{(6,RV;1)}(\mathbf{x}) &= \phi^\dagger(\mathbf{x})\nabla^2\sum_j \nabla_j^4\phi(\mathbf{x}) \\
\mathcal{O}^{(6,RV;2)}(\mathbf{x}) &= \phi^\dagger(\mathbf{x})\sum_j \nabla_j^6\phi(\mathbf{x}).
\end{aligned} \tag{A2}$$

Except for three of these operators which explicitly break the rotational symmetry, they transform as $L = 0$ under rotations.

The operators with one spatial index with up to six derivatives are

$$\begin{aligned}
\mathcal{O}^{(1)}_i(\mathbf{x}) &= \phi^\dagger(\mathbf{x})\nabla_i\phi(\mathbf{x}) \\
\mathcal{O}^{(3)}_i(\mathbf{x}) &= \phi^\dagger(\mathbf{x})\nabla^2\nabla_i\phi(\mathbf{x}) \\
\mathcal{O}^{(5)}_i(\mathbf{x}) &= \phi^\dagger(\mathbf{x})(\nabla^2)^2\nabla_i\phi(\mathbf{x}) \\
\mathcal{O}^{(5,RV)}_i(\mathbf{x}) &= \phi^\dagger(\mathbf{x})\sum_j \nabla_j^4\nabla_i\phi(\mathbf{x}).
\end{aligned} \tag{A3}$$

There is one operator which breaks rotational invariance, and the rest transform as $L = 1$ under rotations.

The operators with two spatial indices with up to six derivatives are

$$\begin{aligned}
\mathcal{O}^{(2)}_{ij}(\mathbf{x}) &= \phi^\dagger(\mathbf{x})\Big[\nabla_i\nabla_j - \frac{1}{3}\delta_{ij}\nabla^2\Big]\phi(\mathbf{x}) \\
\mathcal{O}^{(4)}_{ij}(\mathbf{x}) &= \phi^\dagger(\mathbf{x})\nabla^2\Big[\nabla_i\nabla_j - \frac{1}{3}\delta_{ij}\nabla^2\Big]\phi(\mathbf{x}) \\
\mathcal{O}^{(6)}_{ij}(\mathbf{x}) &= \phi^\dagger(\mathbf{x})(\nabla^2)^2\Big[\nabla_i\nabla_j - \frac{1}{3}\delta_{ij}\nabla^2\Big]\phi(\mathbf{x}) \\
\mathcal{O}^{(6,RV)}_{ij}(\mathbf{x}) &= \phi^\dagger(\mathbf{x})\sum_k \nabla_k^4\Big[\nabla_i\nabla_j - \frac{1}{3}\delta_{ij}\nabla^2\Big]\phi(\mathbf{x}).
\end{aligned} \tag{A4}$$

There is one operator which breaks rotational invariance, and the rest transform as $L = 2$ under rotations.

Operators with three, four, and five spatial indices which have $L = 3$, $L = 4$, and $L = 5$, respectively are listed below. There is no operator which breaks rotational invariance up to six derivatives:

$$\begin{aligned}
\mathcal{O}^{(3)}_{ijk}(\mathbf{x}) &= \phi^\dagger(\mathbf{x})\Big[\nabla_i\nabla_j\nabla_k - \frac{1}{5}\nabla^2(\delta_{ij}\nabla_k + \delta_{jk}\nabla_i + \delta_{ki}\nabla_j)\Big]\phi(\mathbf{x}) \\
\mathcal{O}^{(5)}_{ijk}(\mathbf{x}) &= \phi^\dagger(\mathbf{x})\nabla^2\Big[\nabla_i\nabla_j\nabla_k - \frac{1}{5}\nabla^2(\delta_{ij}\nabla_k + \delta_{jk}\nabla_i + \delta_{ki}\nabla_j)\Big]\phi(\mathbf{x}),
\end{aligned} \tag{A5}$$

$$\begin{aligned}
\mathcal{O}^{(4)}_{ijkl}(\mathbf{x}) = \phi^\dagger(\mathbf{x})\Big[&\nabla_i\nabla_j\nabla_k\nabla_l - \frac{1}{7}\nabla^2(\delta_{ij}\nabla_k\nabla_l + \delta_{ik}\nabla_j\nabla_l + \delta_{il}\nabla_k\nabla_j + \delta_{jk}\nabla_i\nabla_l + \delta_{jl}\nabla_i\nabla_k + \delta_{kl}\nabla_i\nabla_j) \\
&+ \frac{1}{35}(\nabla^2)^2(\delta_{ij}\delta_{kl} + \delta_{ik}\delta_{jl} + \delta_{il}\delta_{jk})\Big]\phi(\mathbf{x}) \\
\mathcal{O}^{(6)}_{ijkl}(\mathbf{x}) = \phi^\dagger(\mathbf{x})\nabla^2\Big[&\nabla_i\nabla_j\nabla_k\nabla_l - \frac{1}{7}\nabla^2(\delta_{ij}\nabla_k\nabla_l + \delta_{ik}\nabla_j\nabla_l + \delta_{il}\nabla_k\nabla_j + \delta_{jk}\nabla_i\nabla_l + \delta_{jl}\nabla_i\nabla_k + \delta_{kl}\nabla_i\nabla_j) \\
&+ \frac{1}{35}(\nabla^2)^2(\delta_{ij}\delta_{kl} + \delta_{ik}\delta_{jl} + \delta_{il}\delta_{jk})\Big]\phi(\mathbf{x}),
\end{aligned} \tag{A6}$$

$$\begin{aligned}
\mathcal{O}^{(5)}_{ijklm}(\mathbf{x}) = \phi^\dagger(\mathbf{x})\Big[&\nabla_i\nabla_j\nabla_k\nabla_l\nabla_m - \frac{1}{7}\nabla^2(\delta_{ij}\nabla_k\nabla_l\nabla_m + \delta_{ik}\nabla_j\nabla_l\nabla_m + \delta_{il}\nabla_k\nabla_j\nabla_m + \delta_{im}\nabla_k\nabla_l\nabla_j + \delta_{jk}\nabla_i\nabla_l\nabla_m \\
&+ \delta_{jl}\nabla_k\nabla_i\nabla_m + \delta_{jm}\nabla_k\nabla_i\nabla_l + \delta_{kl}\nabla_i\nabla_j\nabla_m + \delta_{km}\nabla_i\nabla_j\nabla_l + \delta_{lm}\nabla_i\nabla_j\nabla_k) \\
&+ \frac{1}{63}(\nabla^2)^2[(\delta_{ij}\delta_{kl} + \delta_{ik}\delta_{jl} + \delta_{il}\delta_{jk})\nabla_m + (\delta_{ij}\delta_{km} + \delta_{ik}\delta_{jm} + \delta_{im}\delta_{jk})\nabla_l + (\delta_{ij}\delta_{ml} + \delta_{im}\delta_{jl} + \delta_{il}\delta_{jm})\nabla_k \\
&+ (\delta_{im}\delta_{kl} + \delta_{ik}\delta_{ml} + \delta_{il}\delta_{mk})\nabla_j + (\delta_{mj}\delta_{kl} + \delta_{mk}\delta_{jl} + \delta_{ml}\delta_{jk})\nabla_i]\Big]\phi(\mathbf{x}).
\end{aligned} \tag{A7}$$

Note that as demonstrated in Eq. (A2), there can be more than one operator that breaks rotational invariance at a given order in derivative expansion. To arrive at a notation that is general and useful, one can use the fact that any cubically invariant polynomial of a three-vector $\mathbf{V}$, can be expanded in terms of only three cubically invariant structures,

$$\sum_k V_k^2, \qquad \sum_k V_k^4, \qquad \sum_k V_k^6. \tag{A8}$$

The number of times each structure appears in a derivative operator, as well as the number of free indices, uniquely specifies the operator. For example, with nine derivatives and one spatial index, one can make four independent operators,

$$\begin{aligned}
\mathcal{O}_i^{(4,0,0)}(\mathbf{x}) &= \phi^\dagger(\mathbf{x})(\nabla^2)^4\nabla_i\phi(\mathbf{x})\\
\mathcal{O}_i^{(2,1,0)}(\mathbf{x}) &= \phi^\dagger(\mathbf{x})(\nabla^2)^2\Big(\sum_k\nabla_k^4\Big)\nabla_i\phi(\mathbf{x})\\
\mathcal{O}_i^{(1,0,1)}(\mathbf{x}) &= \phi^\dagger(\mathbf{x})(\nabla^2)\Big(\sum_j\nabla_j^6\Big)\nabla_i\phi(\mathbf{x})\\
\mathcal{O}_i^{(0,2,0)}(\mathbf{x}) &= \phi^\dagger(\mathbf{x})\Big(\sum_k\nabla_k^4\Big)^2\nabla_i\phi(\mathbf{x}),
\end{aligned} \tag{A9}$$

and generally,

$$\mathcal{O}_i^{(m,n,p)}(\mathbf{x}) = (\nabla^2)^m\Big(\sum_k\nabla_k^4\Big)^n\Big(\sum_k\nabla_k^6\Big)^p\nabla_i\phi(\mathbf{x}). \tag{A10}$$

It is then obvious that $d = 2m + 4n + 6p + L$ gives the total number of derivatives in the operator, where L is the number of free indices. For $n = p = 0$, the operator is rotationally invariant with angular momentum L.

APPENDIX B: ROTATIONAL INVARIANCE VIOLATING COEFFICIENTS : AN EXAMPLE

In this appendix, an explicit derivation of a rotational invariance violating coefficient in both coordinate-space, and momentum-space formalism, introduced in Sec. II, is presented. Consider the position-space operator $\hat{\theta}_{00}^{(4)}(\mathbf{x}; a, N)$ where superscript indicates that only operators with four derivatives are retained in the expansion of $\hat{\theta}_{00}$. The goal is to derive the LO correction to the continuum values of coefficients $C_{00,00}^{(4)}$ and $C_{00,00}^{(4;RV)}$:

$$\begin{aligned}
\hat{\theta}_{00}^{(4)}(\mathbf{x}; a, N) &= \phi(\mathbf{x})[(Na)^4C_{00,00}^{(4)}(\nabla^2)^2\\
&\quad + (Na)^4C_{00,00}^{(4;RV)}(\nabla_x^4 + \nabla_y^4 + \nabla_z^4)]\phi(\mathbf{x})\\
&= \frac{3}{4\pi}\frac{(aN)^4}{4!}\sum_{\mathbf{p}}\int_0^1 dyy^6\int d\Omega_{\mathbf{y}}e^{i2\pi N\mathbf{p}\cdot\mathbf{y}}\\
&\quad\times\phi^\dagger(\mathbf{x})(\hat{\mathbf{y}}\cdot\nabla)^4\phi(\mathbf{x})Y_{00}(\Omega_{\mathbf{y}}).
\end{aligned} \tag{B1}$$

The y integration is

$$\begin{aligned}
&\int_0^1 dyy^6\int d\Omega_{\mathbf{y}}e^{i2\pi N\mathbf{p}\cdot\mathbf{y}}y^iy^jy^ky^l\\
&= \alpha(p^ip^jp^kp^l) + \gamma(\delta^{ij}\delta^{kl} + \delta^{ik}\delta^{jl} + \delta^{il}\delta^{jk})\\
&\quad + \beta(p^ip^j\delta^{kl} + p^ip^k\delta^{jl} + p^ip^l\delta^{jk} + p^kp^l\delta^{ij}\\
&\quad + p^jp^l\delta^{ik} + p^jp^k\delta^{il}),
\end{aligned} \tag{B2}$$

and the coefficients α, β, and γ can be determined. It is easy to see that coefficient α makes the dominant contribution in the large N limit. Using

$$\sum_{\mathbf{p}}f(p^2)(\mathbf{p}.\mathbf{A})^4 = \sum_{\mathbf{p}}f(p^2)\Big(\rho|\mathbf{A}|^4 + \sigma\sum_j(A^j)^4\Big), \tag{B3}$$

for any rotational invariant function f of the vector $\mathbf{p}$, with

$$\rho = \frac{1}{2}(|\mathbf{p}|^4 - 3p_z^4), \qquad \sigma = \frac{1}{2}(5p_z^4 - |\mathbf{p}|^4), \tag{B4}$$

one finds that the deviations of $C_{00,00}^{(4)}$ and $C_{00,00}^{(4;RV)}$ from their continuum values are

$$\begin{aligned}
\delta C_{00,00}^{(4)} &= \frac{1}{96\sqrt{\pi}}\sum_{\mathbf{p}\neq\mathbf{0}}\Big(-\frac{3\cos(2\pi N|\mathbf{p}|)}{4\pi^2|\mathbf{p}|^6N^2}\Big)(-3p_z^4 + |\mathbf{p}|^4)\\
\delta C_{00,00}^{(4;RV)} &= \frac{1}{96\sqrt{\pi}}\sum_{\mathbf{p}\neq\mathbf{0}}\Big(-\frac{3\cos(2\pi N|\mathbf{p}|)}{4\pi^2|\mathbf{p}|^6N^2}\Big)(5p_z^4 - |\mathbf{p}|^4).
\end{aligned} \tag{B5}$$

The emergence of rotational invariance violating coefficients from the momentum-space construction is somewhat less obvious. From Eqs. (14) and (15) the operator $\hat{\tilde{\theta}}_{00}^{(4)}(\mathbf{k}; a, N)$ can be written as

$$\begin{aligned}
\hat{\tilde{\theta}}_{00}^{(4)}(\mathbf{k}; a, N) &= \tilde{\phi}(\mathbf{k})\tilde{\phi}(-\mathbf{k})[(Na)^4C_{00,00}^{(4)}|\mathbf{k}|^4 + (Na)^4C_{00,00}^{(4;RV)}(k_x^4 + k_y^4 + k_z^4)]\\
&= \tilde{\phi}(\mathbf{k})\tilde{\phi}(-\mathbf{k})6\sqrt{\pi}\sum_{\mathbf{p}}\sum_{L_1,M_1,L_2,M_2}i^{L_1+L_2}\sqrt{\frac{(2L_1+1)(2L_2+1)}{2L+1}}\langle L_10; L_20|00\rangle\langle L_1M_1; L_2M_2|00\rangle\\
&\quad\times Y_{L_1M_1}(\Omega_{\hat{k}})Y_{L_2M_2}(\Omega_{\hat{p}})\int_0^1 dyy^2j_{L_1}(aN|\mathbf{k}|y)j_{L_2}(2\pi N|\mathbf{p}|y)|_{k^4},
\end{aligned} \tag{B6}$$

where only the terms of order k^4 are retained from the integral. As such, only $L_1 = 4$ with $Y_{4\pm4}(\Omega_{\hat{p}})$ and $Y_{40}(\Omega_{\hat{p}})$, and $L_1 = 0$ with $Y_{00}(\Omega_{\hat{p}})$, contribute to the sum. This reduces the relation to

$$\tilde{\hat{\theta}}^{(4)}_{00}(\mathbf{k};a,N) = 6\sqrt{\pi}\sum_{\mathbf{p}}\Big\{Y_{00}(\Omega_{\hat{k}})Y_{00}(\Omega_{\hat{p}})\int_0^1 dy y^2\frac{(aN|\mathbf{k}|y)^4}{120}j_0(2\pi N|\mathbf{p}|y) + 9[\langle 40;40|00\rangle^2 Y_{40}(\Omega_{\hat{k}})Y_{40}(\Omega_{\hat{p}}) + \langle 40;40|00\rangle\langle 44;4-4|00\rangle Y_{44}(\Omega_{\hat{k}})Y_{4-4}(\Omega_{\hat{p}}) + \langle 40;40|00\rangle\langle 4-4;44|00\rangle Y_{4-4}(\Omega_{\hat{k}})Y_{44}(\Omega_{\hat{p}})] \times\int_0^1 dy y^2\frac{(aN|\mathbf{k}|y)^4}{945}j_4(2\pi N|\mathbf{p}|y)\Big\}. \tag{B7}$$

Using the relations

$$\sum_{\mathbf{p}} f(p^2)(|\mathbf{p}|^4 Y_{40}(\Omega_{\hat{p}})) = \frac{21}{16}\sqrt{\frac{1}{\pi}}\sum_{\mathbf{p}} f(p^2)(5p_z^4 - |\mathbf{p}|^4), \quad \sum_{\mathbf{p}} f(p^2)(|\mathbf{p}|^4 Y_{4\pm4}(\Omega_{\hat{p}})) = \frac{3}{16}\sqrt{\frac{35}{2\pi}}\sum_{\mathbf{p}} f(p^2)(5p_z^4 - |\mathbf{p}|^4), \tag{B8}$$

and keeping the LO term in $1/N$ from the y integration gives

$$\tilde{\hat{\theta}}^{(4)}_{00}(\mathbf{k};a,N) = 3(aN|\mathbf{k}|)^4\sum_{\mathbf{p}\neq\mathbf{0}}\Big(-\frac{\cos(2\pi N|\mathbf{p}|)}{4\pi|\mathbf{p}|^2N^2}\Big)\Big\{\frac{1}{120}Y_{00}(\Omega_{\hat{k}}) + \frac{\sqrt{4\pi}}{945}(5p_z^4 - |\mathbf{p}|^4) \times\Big[\frac{21}{16}\sqrt{\frac{1}{\pi}}Y_{40}(\Omega_{\hat{k}}) + \frac{3}{16}\sqrt{\frac{35}{2\pi}}(Y_{4-4}(\Omega_{\hat{k}}) + Y_{44}(\Omega_{\hat{k}}))\Big]\Big\}. \tag{B9}$$

Finally, we use the relation

$$\frac{k_x^4 + k_y^4 + k_z^4}{|\mathbf{k}|^4} = \frac{6\sqrt{\pi}}{5}Y_{00}(\Omega_{\hat{k}}) + \frac{4\sqrt{\pi}}{15}Y_{40}(\Omega_{\hat{k}}) + \frac{2}{3}\sqrt{\frac{2\pi}{35}}(Y_{4-4}(\Omega_{\hat{k}}) + Y_{44}(\Omega_{\hat{k}})), \tag{B10}$$

to identify the coefficients $\delta C^{(4)}_{00,00}$ and $\delta C^{(4;RV)}_{00,00}$ from Eq. (B9)

$$\delta C^{(4)}_{00,00} = \frac{1}{96\sqrt{\pi}}\sum_{\mathbf{p}\neq\mathbf{0}}\Big(-\frac{3\cos(2\pi N|\mathbf{p}|)}{4\pi^2|\mathbf{p}|^6N^2}\Big)(-3p_z^4 + |\mathbf{p}|^4), \quad \delta C^{(4;RV)}_{00,00} = \frac{1}{96\sqrt{\pi}}\sum_{\mathbf{p}\neq\mathbf{0}}\Big(-\frac{3\cos(2\pi N|\mathbf{p}|)}{4\pi^2|\mathbf{p}|^6N^2}\Big)(5p_z^4 - |\mathbf{p}|^4), \tag{B11}$$

which recovers the position-space results given in Eq. (B5).

APPENDIX C: MATRIX ELEMENTS FOR NONZERO EXTERNAL MOMENTUM

The loop calculations presented in the body of this paper have been performed for vanishing external momentum, therefore only the quantum corrections to the $L = 0$ operator have been considered. In this appendix, the generalization to nonzero external momentum is presented, where the one-loop correction to the two-point function with an insertion of the smeared operator is considered in scalar $g\phi^3$ theory, see Fig. 10. The loop integral to be evaluated is

$$J_{LM} = \frac{3}{4\pi N^3}\sum_{\mathbf{n}}^{|\mathbf{n}|\leq N}\int_{-(\pi/a)}^{\pi/a}\frac{d^4k}{(2\pi)^4} \times\frac{e^{i\mathbf{k}\cdot\mathbf{n}a}}{(\hat{k}^2 + m^2)^2((\widehat{k+P})^2 + m^2)}Y_{LM}(\Omega_{\mathbf{n}}), \tag{C1}$$

where

$$\hat{k}^2 = \frac{4}{a^2}\sum_{\mu}\sin^2\Big(\frac{k_\mu a}{2}\Big), \qquad (\widehat{k+P})^2 = \frac{4}{a^2}\sum_{\mu}\sin^2\Big(\frac{(k_\mu + P_\mu)a}{2}\Big). \tag{C2}$$

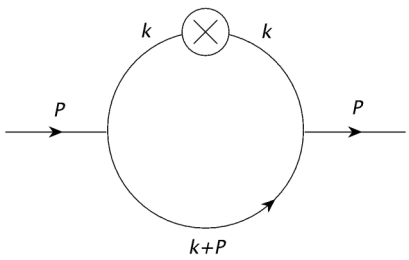

FIG. 10. One-loop contribution to the two-point function with an insertion of the operator in $g\phi^3$

Note that the operator is smeared over a physical region whose size is small compared to the hadronic scale, and as a result the external momenta are small compared to the scale of the operator $\Lambda = 1/Na$. Therefore one may perform a Taylor expansion of the loop integral in P_i/Λ to obtain

$$J_{LM} = \frac{3}{16\pi^4} i^L \frac{1}{\Lambda^2} \int_{-\pi N}^{\pi N} dq_4 d^3q \left[\int_0^1 dy y^2 j_L(qy)\right] Y_{LM}(\Omega_{\mathbf{q}}) \left(4N^2 \sum_{i=1}^{3} \sin^2\left(\frac{q_i}{2N}\right) + 4N^2 \sin^2\left(\frac{q_4}{2N}\right) + \frac{m^2}{\Lambda^2}\right)^{-2}$$
$$\times \left(4N^2 \sum_{i=1}^{3} \sin^2\left(\frac{q_i}{2N}\right) + 4N^2 \sin^2\left(\frac{q_4}{2N} + \frac{P_4}{2N\Lambda}\right) + \frac{m^2}{\Lambda^2}\right)^{-1} \tag{C3}$$
$$\times \sum_{k=0}^{\infty} \left[- \frac{4N^2 \sum_{i=1}^{3} \frac{1}{2} \sin\left(\frac{q_i}{N}\right) \sin\left(\frac{P_i}{N\Lambda}\right) + 4N^2 \sum_{i=1}^{3} \cos\left(\frac{q_i}{N}\right) \sin^2\left(\frac{P_i}{2N\Lambda}\right)}{4N^2 \sum_{i=1}^{3} \sin^2\left(\frac{q_i}{2N}\right) + 4N^2 \sin^2\left(\frac{q_4}{2N} + \frac{P_4}{2N\Lambda}\right) + \frac{m^2}{\Lambda^2}} \right]^k,$$

where $\mathbf{q} = \mathbf{k}/\Lambda$, $q_4 = k_4/\Lambda$, and only the leading term in the Poisson sum is retained. As was shown before, the nonzero terms in the Poisson sum are suppressed by at least $1/N^2$ compared to the continuum operator insertion in the loop.

The first term in the above Taylor expansion corresponds to the zero external momentum in the loop, therefore at LO, it contributes to the $L = 0$ operator, and the subleading rotational invariance breaking operators can be easily shown to be suppressed by $1/N^2$ using the procedure described in Sec. II B. Note that the loop integrals one needs to deal with in $g\phi^3$ are more convergent than comparable integrals in $\lambda\phi^4$ theory, which simplifies the discussion of the scaling of the different contributions.

The next term in the Taylor expansion of the loop integral can be expanded in large N since the integral is convergent. The numerator has an expansion of the form

$$\begin{aligned} \text{Num.} &\sim 4N^2 \sum_{i=1}^{3} \frac{1}{2} \sin\left(\frac{q_i}{N}\right) \sin\left(\frac{P_i}{N\Lambda}\right) \\ &\quad + 4N^2 \sum_{i=1}^{3} \cos\left(\frac{q_i}{N}\right) \sin^2\left(\frac{P_i}{2N\Lambda}\right) \\ &= \frac{2\mathbf{P}\cdot\mathbf{q}}{\Lambda} + \frac{|\mathbf{P}|^2}{\Lambda^2} + \mathcal{O}\left(\frac{1}{N^2}\right), \end{aligned} \tag{C4}$$

where the rotational invariance breaking terms are suppressed by at least $1/N^2$, and the leading contribution to the above integral modifies the $L = 1$ matrix element, while the $L = 0$ term is suppressed by $1/\Lambda$ compared to the $L = 1$ contribution. The next terms in the Taylor expansion give rise to contributions to the $L = 2, 3, \ldots$ matrix elements at the LO in $1/\Lambda$, while the rotational invariance violating terms remain suppressed by at least $1/N^2$ compared to the LO contributions.

APPENDIX D: LINKS ON THE GRID

In this appendix, the method to evaluate the link at $\mathcal{O}(g)$ on a three-dimensional grid is outlined through an example, and the result is generalized to other similar cases. The link is constructed to be the closest link to the continuum diagonal link in the continuum.

Suppose that the link lies between points x and $x + \mathbf{n}a$ on a cubic lattice where: $\mathbf{n}a = a_0(Q, 1, 0)$. Q is an arbitrary integer and a_0 is a finite number denoting the original lattice spacing which is not necessarily small. Then the paths which make minimal area with the diagonal path can be formed easily. Among those, the paths which are symmetric under reflection around the midpoint of the path are desired since they have somewhat simple forms. One such path is shown in Fig. 8(a) for $Q = 2$, where it is straightforward to show that:

$$U^{(1g)}_{(Q,1,0)}(q) = iga_0 e^{i\mathbf{q}\cdot\mathbf{n}a/2} \left[A_y(q) + 2A_x(q) \frac{\sin(Qq_xa_0/4)}{\sin(q_xa_0/2)} \times \cos\left(\frac{Qq_xa_0}{4} + \frac{q_ya_0}{2}\right)\right]. \tag{D1}$$

If the lattice spacing is halved, the closest link to the diagonal path can be obtained by adding up two paths each of the form above with an appropriate phase factor and where $\mathbf{n}a$ is replaced by $\mathbf{n}a/2$, Fig. 8(b),

$$U^{(1g)}_{(Q,1,0)}(q) = ig\frac{a_0}{2} e^{i\mathbf{q}\cdot\mathbf{n}a/2} \frac{\sin\left(\frac{\mathbf{q}\cdot\mathbf{n}a}{2}\right)}{\sin\left(\frac{\mathbf{q}\cdot\mathbf{n}a}{4}\right)} \left[A_y(q) + 2A_x(q) \times \frac{\sin(Qq_xa_0/8)}{\sin(q_xa_0/4)} \cos\left(\frac{Qq_xa_0}{8} + \frac{q_ya_0}{4}\right)\right]. \tag{D2}$$

This process can be repeated to build extended gauge links on finer grids. For the general case, where the original lattice spacing is divided by 2^K, it is not hard to show that

$$U^{(1g)}_{2^K(Q,1,0)}(q) = ig\frac{a_0}{2^K} e^{i\mathbf{q}\cdot\mathbf{n}a/2} \frac{\sin\left(\frac{\mathbf{q}\cdot\mathbf{n}a}{2}\right)}{\sin\left(\frac{\mathbf{q}\cdot\mathbf{n}a}{2^{K+1}}\right)} \left[A_y(q) + 2A_x(q) \times \frac{\sin(Qq_xa_0/2^{K+2})}{\sin(q_xa_0/2^{K+1})} \cos\left(\frac{Qq_xa_0}{2^{K+2}} + \frac{q_ya_0}{2^{K+1}}\right)\right]. \tag{D3}$$

The continuum limit is obtained by taking $K \to \infty$, which corresponds to $a = a_0/2^K \to 0$, recovering Eq. (40). Note that after interchanging the gauge field indices properly, this expression is applicable to a class of $\mathbf{n}$ vectors with one zero component and $n_i/n_j = Q$ for the ratio of the remaining components.

The above expression for the gauge link in Eq. (D3) can be generalized easily to another class of $\mathbf{n}$ vectors with one component being equal to Q and the other two components each being one. For example for $\mathbf{n}a = a_0(Q, 1, 1)$ one obtains

$$U^{(1g)}_{2^K(Q,1,1)}(q) = ig\frac{a_0}{2^K}e^{i\mathbf{q}\cdot\mathbf{n}a/2}\frac{\sin(\frac{\mathbf{q}\cdot\mathbf{n}a}{2})}{\sin(\frac{\mathbf{q}\cdot\mathbf{n}a}{2^{K+1}})}\Big[A_z(q)e^{iq_ya_0/2^{K+1}} + A_y(q)e^{-iq_za_0/2^{K+1}} + 2A_x(q)\frac{\sin(Qq_xa_0/2^{K+2})}{\sin(q_xa_0/2^{K+1})}\cos\Big(\frac{Qq_xa_0}{2^{K+2}} + \frac{q_ya_0}{2^{K+1}} + \frac{q_za_0}{2^{K+1}}\Big)\Big]. \tag{D4}$$

However, since the vector $\mathbf{n}a$ is symmetric in its y and z components, the link has to respect this symmetry as well. In fact, there exist an equivalent path which arises from the first path by interchanging the steps in the y direction and the z direction. Taking an average of these two paths gives a link which is symmetric in the y and z components,

$$\bar{U}^{(1g)}_{2^K(Q,1,1)}(q) = ig\frac{a_0}{2^K}e^{i\mathbf{q}\cdot\mathbf{n}a/2}\frac{\sin(\frac{\mathbf{q}\cdot\mathbf{n}a}{2})}{\sin(\frac{\mathbf{q}\cdot\mathbf{n}a}{2^{K+1}})}\Big[A_z(q)\cos\Big(\frac{q_ya_0}{2^{K+1}}\Big) + A_y(q)\cos\Big(\frac{q_za_0}{2^{K+1}}\Big) + 2A_x(q)\frac{\sin(Qq_xa_0/2^{K+2})}{\sin(q_xa_0/2^{K+1})}\cos\Big(\frac{Qq_xa_0}{2^{K+2}} + \frac{q_ya_0}{2^{K+1}} + \frac{q_za_0}{2^{K+1}}\Big)\Big]. \tag{D5}$$

Taking the $K \to \infty$ limit of the above link gives rise to the rotational invariant link as well as noncontinuum corrections which start at $\mathcal{O}(a^2)$.

Another class of $\mathbf{n}$ vectors are those where two components are equal to Q while the other one is equal to one. For example for $\mathbf{n}a = a_0(Q, Q, 1)$ the link which is symmetric with respect to x and y can be shown to have the form:

$$\bar{U}^{(1g)}_{2^K(Q\times Q\times 1)} = ig\frac{a_0}{2^K}e^{i\mathbf{q}\cdot\mathbf{\Delta x}/2}\frac{\sin(\frac{\mathbf{q}\cdot\mathbf{\Delta x}}{2})}{\sin(\frac{\mathbf{q}\cdot\mathbf{\Delta x}}{2^{K+1}})}\Big[2\Big(A_x(q)\cos\Big(\frac{q_ya_0}{2^{K+1}}\Big) + A_y(q)\cos\Big(\frac{q_xa_0}{2^{K+1}}\Big)\Big)\frac{\sin(Q(q_xa_0 + q_ya_0)/2^{K+2})}{\sin((q_xa_0 + q_ya_0)/2^{K+1})} \times \cos\Big(\frac{Qq_xa_0}{2^{K+2}} + \frac{Qq_ya_0}{2^{K+2}} + \frac{q_za_0}{2^{K+1}}\Big) + A_z(q)\Big], \tag{D6}$$

where $\bar{U}$ the average of two links which are identical upon interchanging the x and y coordinate axes. This link recovers the rotational invariant link up to corrections of $\mathcal{O}(a^2)$.

For $\mathbf{n}$ vectors with equal components, $\mathbf{n}a = a_0(Q, Q, Q)$, there are six equivalent links which are averaged over to obtain

$$\bar{U}^{(1g)}_{2^K(Q\times Q\times Q)} = ig\frac{a_0}{2^K}e^{i\mathbf{q}\cdot\mathbf{\Delta x}/2}\frac{\sin(\frac{\mathbf{q}\cdot\mathbf{\Delta x}}{2})}{\sin(\frac{\mathbf{q}\cdot\mathbf{\Delta x}}{2^{K+1}})}\Big[2\Big(A_x(q)\cos\Big(\frac{q_ya_0}{2^{K+1}} + \frac{q_za_0}{2^{K+1}}\Big) + A_y(q)\cos\Big(\frac{q_xa_0}{2^{K+1}} + \frac{q_za_0}{2^{K+1}}\Big) + A_z(q)\cos\Big(\frac{q_xa_0}{2^{K+1}} + \frac{q_ya_0}{2^{K+1}}\Big)\Big)\frac{\sin((Qq_xa_0 + Qq_ya_0 + Qq_za_0)/2^{K+2})}{\sin((q_xa_0 + q_ya_0 + q_za_0)/2^{K+1})}\cos\Big(\frac{Qq_xa_0}{2^{K+2}} + \frac{Qq_ya_0}{2^{K+2}} + \frac{Qq_za_0}{2^{K+2}}\Big)\Big], \tag{D7}$$

which results in $\mathcal{O}(a^2)$ corrections to the rotational invariant continuum path. It is the case that determining the link for a general extended path is quite involved, but the general trend that the deviation from the rotationally invariant continuum path is $\mathcal{O}(a^2)$ is anticipated.

[1] K. G. Wilson, Phys. Rev. D **10**, 2445 (1974).
[2] K. Symanzik, Nucl. Phys. **B226**, 187 (1983).
[3] K. Symanzik, Nucl. Phys. **B226**, 205 (1983).
[4] G. Parisi, Nucl. Phys. **B254**, 58 (1985).
[5] C. Lang and C. Rebbi, Phys. Lett. **115B**, 137 (1982).
[6] C. Lang, Phys. Lett. B **229**, 97 (1989).
[7] C. Lang and U. Winkler, Phys. Rev. D **47**, 4705 (1993).
[8] P. Weisz, Nucl. Phys. **B212**, 1 (1983).
[9] P. Weisz and R. Wohlert, Nucl. Phys. **B236**, 397 (1984).
[10] M. Luscher and P. Weisz, Nucl. Phys. **B240**, 349 (1984).

[11] G. Curci, P. Menotti, and G. Paffuti, Phys. Lett. **130B**, 205 (1983).
[12] H. W. Hamber and C. M. Wu, Phys. Lett. **133B**, 351 (1983).
[13] T. Eguchi and N. Kawamoto, Nucl. Phys. **B237**, 609 (1984).
[14] W. Wetzel, Phys. Lett. **136B**, 407 (1984).
[15] B. Sheikholeslami and R. Wohlert, Nucl. Phys. **B259**, 572 (1985).
[16] R. Johnson, Phys. Lett. **114B**, 147 (1982).
[17] B. Berg and A. Billoire, Nucl. Phys. **B221**, 109 (1983).
[18] J. E. Mandula, G. Zweig, and J. Govaerts, Nucl. Phys. **B228**, 91 (1983).
[19] H.-W. Lin, Chin. J. Phys. (Taipei) **49**, 827 (2011).
[20] T. Burch, C. Gattringer, L. Y. Glozman, C. Hagen, C. Lang *et al.*, Phys. Rev. D **73**, 094505 (2006).
[21] C. Gattringer, L. Y. Glozman, C. Lang, D. Mohler, and S. Prelovsek, Phys. Rev. D **78**, 034501 (2008).
[22] R. G. Petry, D. Harnett, R. Lewis, and R. Woloshyn, Phys. Rev. D **78**, 074502 (2008).
[23] T. Burch, C. Hagen, M. Hetzenegger, and A. Schafer, Phys. Rev. D **79**, 114503 (2009).
[24] J. J. Dudek, R. G. Edwards, M. J. Peardon, D. G. Richards, and C. E. Thomas, Phys. Rev. Lett. **103**, 262001 (2009).
[25] J. J. Dudek, R. G. Edwards, M. J. Peardon, D. G. Richards, and C. E. Thomas, Phys. Rev. D **82**, 034508 (2010).
[26] R. G. Edwards, J. J. Dudek, D. G. Richards, and S. J. Wallace, Phys. Rev. D **84**, 074508 (2011).
[27] S. Meinel, Phys. Rev. D **85**, 114510 (2012).
[28] S. Basak *et al.* (Lattice Hadron Physics Collaboration (LHPC)), Phys. Rev. D **72**, 074501 (2005).
[29] C. Allton *et al.* (UKQCD Collaboration), Phys. Rev. D **47**, 5128 (1993).
[30] C. Morningstar and M. J. Peardon, Phys. Rev. D **69**, 054501 (2004).
[31] M. Peardon *et al.* (Hadron Spectrum Collaboration), Phys. Rev. D **80**, 054506 (2009).
[32] H. B. Meyer and M. J. Teper, Nucl. Phys. **B658**, 113 (2003).
[33] R. W. Johnson, Phys. Rev. D **66**, 074502 (2002).
[34] M. J. Teper, Phys. Rev. D **59**, 014512 (1998).
[35] S. Capitani and G. Rossi, Nucl. Phys. **B433**, 351 (1995).
[36] G. Beccarini, M. Bianchi, S. Capitani, and G. Rossi, Nucl. Phys. **B456**, 271 (1995).
[37] M. Gockeler, R. Horsley, E.-M. Ilgenfritz, H. Perlt, P. E. Rakow, G. Schierholz, and A. Schiller, Phys. Rev. D **54**, 5705 (1996).
[38] M. Gockeler, R. Horsley, E.-M. Ilgenfritz, H. Perlt, P. E. Rakow G. Schierholz, and A. Schiller, Nucl. Phys. **B472**, 309 (1996).
[39] M. Gockeler, R. Horsley, W. Kurzinger, H. Oelrich, D. Pleiter, P. E. L. Rakow, A. Schäfer, and G. Schierholz, Phys. Rev. D **63**, 074506 (2001).
[40] M. Gockeler, R. Horsley, D. Pleiter, P. E. Rakow, and G. Schierholz (QCDSF Collaboration), Phys. Rev. D **71**, 114511 (2005).
[41] M. Gockeler, R. Horsley, B. Klaus, D. Pleiter, P. E. L. Rakow, S. Schaefer, A. Schäfer, and G. Schierholz, Nucl. Phys. **B623**, 287 (2002).
[42] M. Gockeler, R. Horsley, D. Pleiter, P. E. Rakow, A. Schafer, G. Schierholz, H. Stüben, and J. M. Zanotti, Phys. Rev. D **72**, 054507 (2005).
[43] G. Martinelli and C. T. Sachrajda, Phys. Lett. B **196**, 184 (1987).
[44] G. Martinelli and C. T. Sachrajda, Nucl. Phys. **B306**, 865 (1988).
[45] G. Martinelli and C. T. Sachrajda, Nucl. Phys. **B316**, 355 (1989).
[46] C. Dawson, G. Martinelli, G. C. Rossi, C. T. Sachrajda, S. Sharpe, M. Talevi, and M. Testa, Nucl. Phys. **B514**, 313 (1998).
[47] W. Detmold and C. D. Lin, Phys. Rev. D **73**, 014501 (2006).
[48] M. Campostrini, A. Pelissetto, P. Rossi, and E. Vicari, Europhys. Lett. **38**, 577 (1997).
[49] M. Campostrini, A. Pelissetto, P. Rossi, and E. Vicari, Phys. Rev. E **57**, 184 (1998).
[50] G. P. Lepage and P. B. Mackenzie, Phys. Rev. D **48**, 2250 (1993).
[51] T. Luu and M. J. Savage, Phys. Rev. D **83**, 114508 (2011).